

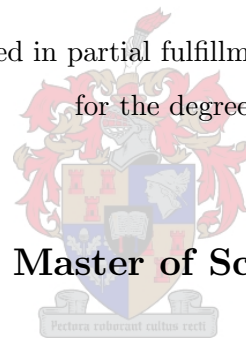
Determining non-linear optical properties using the Z-scan technique

by

Pieter Neethling

Thesis presented in partial fulfillment of the requirements

for the degree of



Master of Science

at the University of Stellenbosch

Supervisor:

Dr. E.G. Rohwer

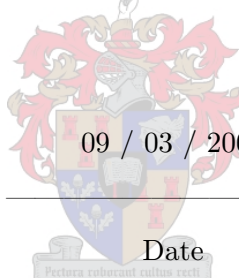
April 2005

Declaration

I, the undersigned, hereby declare that the work contained in this thesis is my own original work and that I have not previously in its entirety or in part submitted it at any university for a degree.



Signature



09 / 03 / 2005

Date

Pectora roborant cultus recti

Abstract

The extremely high light intensities produced by lasers and the increasing use of lasers highlights the need for measures to prevent damage to materials due to exposure to high intensity laser light. In particular it necessitates the development of systems to protect optical sensors, including the human eye. In this work optical limiters were investigated as a system for protecting sensors. An optical limiter transmits ambient light, but absorbs high intensity light. This makes it ideal for protecting sensors from laser radiation, since it allows the sensor to operate unhindered at design intensities while protecting it from harmful high intensity radiation.

There are various mechanisms used for optical limiting, and in this work the nonlinear absorption and the nonlinear index of refraction changes of materials were investigated. A facility was established to measure the nonlinear optical properties of a variety of materials, in order to classify them as possible optical limiters. This entailed creating a so called Z-scan setup, which enabled us to measure the nonlinear absorption coefficient and the nonlinear index of refraction of a material. The theory and the design of the setup are discussed and experimental results obtained using this setup are presented.

A wide variety of material types were investigated to show the versatility of the experimental setup. These included C_{60} , which was analyzed in solution; ZnO which is a crystal; CdS quantum dots in solution; and poly(dioctyl-fluorene), which is a large polymer molecule, in solution. The materials investigated in this work were chosen based on their known strong nonlinear optical properties. Emphasis was placed on measuring the nonlinear absorption coefficients since it was the dominant optical limiting effect of the materials under investigation.

The results obtained displayed the same trends as published results and it shows that the established facility was capable of measuring the nonlinear properties of these samples. The experimental limitations of the setup were determined, and critical experimental parameters were identified for measurements of this nature. Improvements to the experimental facility are suggested to improve the accuracy of future measurements.

Opsomming

Die besonder hoë ligintensiteite wat deur lasers genereer word en die toenemende gebruik van lasers beklemtoon die noodsaaklikheid vir maatreëls om die beskadiging van materiale deur blootstelling aan die hoë intensiteit laserlig te bekamp. In die besonder noodsaak dit die ontwikkeling van sisteme om optiese sensors te beskerm, insluitende die menslike oog. In hierdie werk word optiese beperkers ("optical limiters") ondersoek as moontlike sensor beskermers. 'n Optiese beperker laat lae intensiteit lig deur, maar absorbeer hoër intensiteit lig. Hierdie eienskap maak beperkers ideale beskermers teen laserlig, omdat die sensors ongehinderd kan funksioneer by ontwerp-intensiteite terwyl dit die sensor beskerm teen nadelige hoë intensiteit straling.

Daar is verskeie meganismes wat gebruik kan word vir optiese beperking, en in hierdie werk word nie-liniêre absorpsie en veranderinge in die nie-liniêre brekingsindeks van materiale ondersoek as moontlike meganismes. Dit het die opbou van 'n sogenaamde Z-skanderingsopstelling behels, wat dit moontlik gemaak het om die nie-liniêre absorpsie koëffisiënt en nie-liniêre brekingsindeks van 'n materiaal te meet. Die teorie en die ontwerp van die opstelling word bespreek, en die eksperimentele resultate verkry word voorgestel.

'n Wye verskeidenheid van materiaalsoorte is ondersoek om die veelsydigheid van die opstelling ten toon te stel. Dit sluit in C_{60} , wat in oplossing ondersoek is; ZnO wat 'n kristal is; CdS kwantum "dots" in oplossing; en poly(dioctyl-fluorene), wat 'n groot polimeer molekule is, in oplossing. Die materiale wat in die werk ondersoek is, is gekies op grond van hul bekende hoë nie-liniêre optiese eienskappe. Daar is klem gelê op die meet van nie-liniêre absorpsie koëffisiënte omdat dit die dominante optiese beperkende effek van die materiale was wat ondersoek is.

Die resultate wat verkry is, is met gepubliseerde waardes vergelyk en dit het daarop gedui dat die nuut daargestelde fasiliteit geskik is om die nie-liniêre optiese eienskappe van die gekose materiale vas te stel. Die eksperimentele beperkings van die opstelling is bepaal, en die kritieke eksperimentele parameters vir die tipe metings is geïdentifiseer. Verbeteringe aan die eksperimentele fasiliteit, om die akkuraatheid van toekomstige metings te verhoog, word voorgestel.

Acknowledgements

I would like to thank the following people:

- Dr. E.G. Rohwer for his supervision of this work and the immeasurable guidance and assistance along with countless useful discussions.
- Prof. P.E. Walters for contributing his knowledge and experience to the project.
- Mr. U. Deutschländer for all his technical assistance that he lent to the project.
- Mr. M. Bartolini for his electronic and software support.
- All my colleagues, especially Anton and Torsten, who could always be counted upon to give advice and to listen to problems.
- All the other members of the Laser Research Institute for the useful discussions.
- My friends and family for their faith and support.

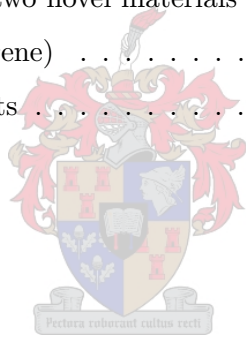
My studies were funded by the National Research Foundation and the National Laser Centre (CSIR). The project was funded by DefenceTek (CSIR).



Contents

1	Problem statement and overview	1
1.1	Introduction and problem statement	1
1.2	Aim	2
2	Theory of nonlinear optical processes in matter	4
2.1	Theoretical framework for nonlinear light-matter interactions	4
2.2	Self focusing (nonlinear refraction)	11
2.2.1	Conditions for self focusing	14
2.3	Nonlinear absorption	15
3	The Z-scan as analysis technique	18
3.1	The Z-scan	18
3.2	Theory	22
3.2.1	Nonlinear refraction	22
3.2.2	Nonlinear absorption	28
4	Experimental setup and considerations of the Z-scan technique	33
4.1	Refinement of experimental setup	33
4.2	Experimental setup	35
4.3	Characterization of the experimental setup	36
4.3.1	Beam quality	37
4.3.2	Data capturing, processing and averaging	40
4.3.3	Sample thickness	44

4.3.4	Background	44
4.3.5	Solvent effect	45
4.3.6	Nonlinear refraction in cuvette material (quartz)	45
4.3.7	Stray reflections	45
4.3.8	Optical damage in cuvette	46
4.3.9	Nonlinear scattering	46
4.3.10	Cuvette type	47
4.3.11	Iris for closed aperture Z-scans	48
5	Material descriptions and experimental results	49
5.1	C ₆₀ , the Buckminsterfullerene	50
5.1.1	Nonlinear absorption in C ₆₀	50
5.1.2	Experimental results for C ₆₀	52
5.2	Experimental results for single crystalline ZnO	59
5.3	Experimental results of two novel materials	62
5.3.1	Poly(dioctyl-fluorene)	63
5.3.2	CdS quantum dots	66
6	Conclusions	68
	Appendix	70



List of Figures

1-1	An ideal optical limiter.	2
2-1	Harmonic and general potential curves.	6
2-2	Self focusing of a Gaussian beam.	13
2-3	A schematic graph depicting linear absorption.	17
2-4	A schematic graph depicting pure two-photon absorption.	17
3-1	The basic Z-scan setup.	19
3-2	Gaussian beam interacting with a nonlinear sample.	20
3-3	Traces showing nonlinear refraction.	20
3-4	Obtaining the resultant nonlinear refraction graph.	21
3-5	A Gaussian beam propagating through a nonlinear sample.	22
3-6	A graph illustrating the meaning of ΔT_{p-v}	27
3-7	A graph depicting the lowest possible useful transmittance.	31
3-8	The variation of $T(z)$ with m	32
4-1	The final Z-scan setup used in the experiments.	35
4-2	An intensity profile of the Dye laser pulse.	37
4-3	Open aperture Z-scan using the spatially filtered laser beam.	38
4-4	Spatially filtered Dye laser beam.	39
4-5	Creation of a clipped Airy pattern.	39
4-6	Intensity profiles of the clipped Airy pattern.	40
4-7	The energy distribution as measured by the reference detector.	42
4-8	The energy distribution as measured by the probe detector.	42

4-9	Reference measurements and corresponding probe measurements.	43
4-10	A Z-scan showing nonlinear scattering.	47
5-1	The structure of a C ₆₀ molecule.	50
5-2	An energy diagram of the C ₆₀ molecule.	51
5-3	An open aperture Z-scan conducted with toluene.	54
5-4	A Z-scan of C ₆₀	55
5-5	The dependence of β on C ₆₀ concentration.	55
5-6	An open aperture Z-scan performed on C ₆₀	57
5-7	A closed aperture Z-scan performed on C ₆₀	57
5-8	The resultant nonlinear index of refraction data for C ₆₀	58
5-9	A closed aperture Z-scan of toluene.	59
5-10	A closed aperture Z-scan of ZnO.	60
5-11	An open aperture Z-scan of ZnO.	61
5-12	A closed aperture Z-scan of ZnO.	61
5-13	The resultant nonlinear index of refraction data for ZnO.	62
5-14	The monomer of poly(dioctyl-fluorene).	63
5-15	An open aperture Z-scan of poly(dioctyl-fluorene).	64
5-16	The time-dependent transmittance of poly(dioctyl-fluorene).	65
5-17	Two Z-scans of poly(dioctyl-fluorene) after oxidation.	66
5-18	An open aperture Z-scan of CdS quantum dots.	67

Chapter 1

Problem statement and overview

1.1 Introduction and problem statement

Since the advent of the laser in the 1960s, the study of nonlinear optical properties of materials has become readily accessible. However, along with the laser came all the dangers associated with high intensity light, including damage to optical sensors like the human eye, range finders and night vision equipment. This necessitates the protection of these sensors from laser light. Industry is continually looking for materials that transmit light of low intensities (ambient light) but absorb harmful high intensity light (laser radiation). These materials are known as optical limiters. The working of an ideal optical limiter can be seen in Figure 1-1. As the incident light intensity increases, the transmitted light reaches a threshold value at which point it is clamped. Optical limiters are gaining in importance as lasers, in both commercial and military applications, become more commonplace.

When considering a material as an optical limiter, two of the properties that are of particular interest are the material's nonlinear absorption coefficient and its nonlinear index of refraction. Both change the intensity of the light in a nonlinear way as it passes through the medium. By measuring these nonlinear properties of materials, these materials can be identified as possible optical limiters.

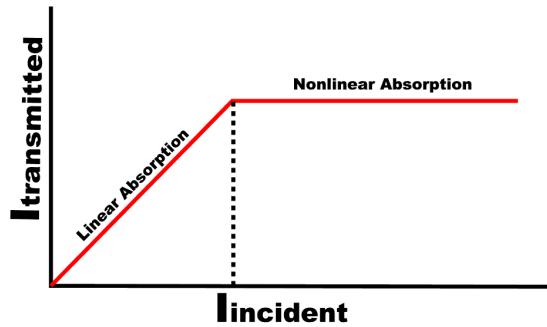


Figure 1-1: A schematic representation of the transmission through an ideal optical limiter.

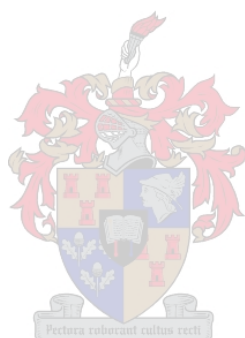
When considering the processes that contribute to the optical limiting behaviour of a material, the process that best attenuates a laser beam, and thus protects an optical sensor, is nonlinear absorption. The other processes like nonlinear refraction and nonlinear scattering, to name but two, are merely secondary in importance. This implies that when a material is identified as a possible optical limiter, it is its nonlinear absorption coefficient that will determine whether or not it will act as an effective optical limiter. To this end it is necessary to construct a setup by means of which the nonlinear absorption coefficient can be measured.

1.2 Aim

The aim of this project was two-fold. The first was to conduct a theoretical investigation into the nonlinear properties of materials and the mechanisms governing these properties. This investigation focussed on nonlinear absorption and nonlinear refraction. Accompanying this, a theoretical investigation into the Z-scan technique, used to measure the nonlinear index of refraction and the nonlinear absorption coefficient, was performed.

The second aim was to establish a Z-scan facility, which would enable the measurement of the nonlinear absorption coefficients and the nonlinear indices of refraction of a host of materials. This entailed determining whether the capabilities for performing these measurements could be established and, if so, to assemble the setup and evaluate it. Particular emphasis was placed on

determining the factors that influenced repeatable measurements. This was to ensure that the setup was reliable and would enable the future investigation of novel materials for evaluation as possible optical limiters. The scope of the project did not extend to the search for possible optical limiters, although the versatility of the setup needed to be demonstrated, and this was done by measuring the nonlinear properties of a range of completely different materials.



Chapter 2

Theory of nonlinear optical processes in matter

For a discussion of nonlinear processes in materials, it is necessary to have a general theoretical understanding of these processes. In this chapter a concise framework of this theory, starting from Maxwell's equations, is presented.

2.1 Theoretical framework for nonlinear light-matter interactions

It is customary to start with Maxwell's equations when describing any light-matter interaction.

$$\nabla \times \mathbf{H} = \frac{\partial \mathbf{D}}{\partial t} \quad (2.1)$$

$$\nabla \cdot \mathbf{D} = 0 \quad (2.2)$$

$$\nabla \times \mathbf{E} = -\frac{\partial \mathbf{B}}{\partial t} \quad (2.3)$$

$$\nabla \cdot \mathbf{H} = 0 \quad (2.4)$$

In these equations it has been assumed that the surface charge density, σ , and the volume charge density, ρ , are both zero. It is important to note that the magnetic field, \mathbf{B} , and \mathbf{H} are related through $\mathbf{B} = \mu_0 \mathbf{H}$, μ_0 being the permeability of free space, and that the electric

field, \mathbf{E} , and the electric displacement, \mathbf{D} , are related through $\mathbf{D}(\mathbf{E}) = \epsilon_0\mathbf{E} + \mathbf{P}(\mathbf{E})$, where the dielectric polarization $\mathbf{P}(\mathbf{E})$ is the dipole moment per unit volume, and ϵ_0 is the permittivity of free space.

Light-matter interactions are usually considered within the framework of the Lorentz model [1]. In the Lorentz model, the electrons are considered to be bound to the atom in a harmonic potential. This is equivalent to expressing the polarization of the material as a result of an electric field as

$$\mathbf{P}(\mathbf{E}) = \epsilon_0\chi^{(1)}\mathbf{E} \quad (2.5)$$

where $\chi^{(1)}$ is the linear susceptibility of the material. This accounts accurately for all linear phenomena occurring during light-matter interactions. This, however, does not explain the nonlinear phenomena observed when high intensity light interacts with matter. To explain this, it is necessary to consider the electron to be bound in a more generalized potential, namely an anharmonic potential, which is approximated by a harmonic potential at low energies. For this discussion the approach of Milonni and Eberly [1] is followed. This general potential (see Figure 2-1) is normally expressed as a power series

$$V(x) = \frac{1}{2}m\omega_0^2x^2 + Ax^3 + Bx^4 + \dots \quad (2.6)$$

in which the first term is the harmonic potential, which dominates the expression for small displacements, x . This can be obtained in the following way. Whatever the true potential is, it can be expanded in a Taylor series in the normal fashion

$$V(x) = V(0) + x \left(\frac{dV}{dx} \right)_{x=0} + \frac{1}{2!}x^2 \left(\frac{d^2V}{dx^2} \right)_{x=0} + \frac{1}{3!}x^3 \left(\frac{d^3V}{dx^3} \right)_{x=0} + \dots \quad (2.7)$$

about the equilibrium point, $x = 0$. $V(0)$ is just an additive constant to the total energy and does not give rise to any force ($F = -dV/dx$). The constant term can therefore be neglected. It can be seen from Figure 2-1 that

$$\left(\frac{dV}{dx} \right)_{x=0} = 0 \quad (2.8)$$

and that

$$\left(\frac{d^2V}{dx^2}\right)_{x=0} > 0 . \quad (2.9)$$

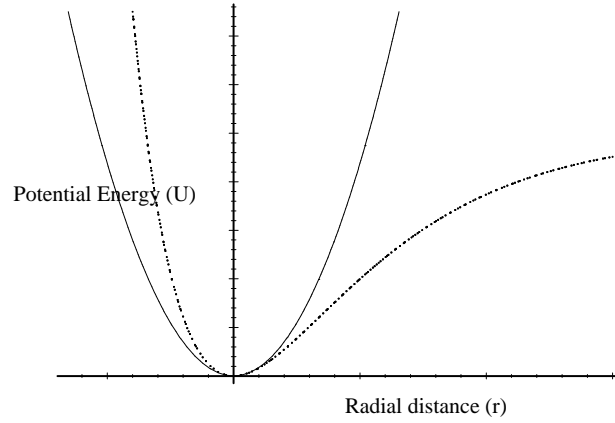


Figure 2-1: Curves indicating a harmonic potential (solid line) and a generalised potential (dashed line).

The result is that Equation 2.7 can be rewritten as

$$V(x) = \frac{1}{2}x^2 \left(\frac{d^2V}{dx^2}\right)_{x=0} + \frac{1}{6}x^3 \left(\frac{d^3V}{dx^3}\right)_{x=0} + \dots \quad (2.10)$$

and since $d^2V/dx^2 > 0$, we can define

$$m\omega_0^2 \equiv \left(\frac{d^2V}{dx^2}\right)_{x=0} . \quad (2.11)$$

In a similar fashion we define

$$A \equiv \frac{1}{6} \left(\frac{d^3V}{dx^3}\right)_{x=0} . \quad (2.12)$$

This can be done for all the terms in Equation 2.6.

The force on an electron in this potential is given by

$$\mathbf{F} = -\frac{dV}{dx} = -m\omega_0^2x - 3Ax^2 - 4Bx^3 - \dots \quad (2.13)$$

which implies

$$\ddot{x} + \omega_0^2 x + \frac{3A}{m} x^2 + \frac{4B}{m} x^3 + \dots = \frac{e}{m} \mathbf{E}(t) \quad (2.14)$$

when considering Newton's equations of motion. This is a nonlinear differential equation, which is generally not possible to solve analytically.

The polarization density, \mathbf{P} , is given by

$$\mathbf{P} = Ne\hat{x} \quad (2.15)$$

where N is the number of molecules per unit volume. Considering potential solutions for Equation 2.14 and substituting them into Equation 2.15 leads to a power series in \mathbf{E} for the polarization, \mathbf{P} [2].

$$\mathbf{P}(\mathbf{E}) = \epsilon_0(\chi^{(1)}\mathbf{E} + \chi^{(2)}\mathbf{E}\mathbf{E} + \chi^{(3)}\mathbf{E}\mathbf{E}\mathbf{E} + \dots) \quad (2.16)$$

The expansion coefficients, $\chi^{(n)}$, are tensors (Equation 2.16 therefore represents a tensor product) and are the dielectric susceptibilities which are intrinsic properties of the material. As was mentioned, $\chi^{(1)}$ is the linear susceptibility. It is a complex number that governs the linear optical processes in the material, the real part being related to the linear index of refraction, n , and the imaginary part related to the linear absorption coefficient, α . All the other $\chi^{(n)}$ are the higher order susceptibilities that govern the nonlinear processes. They are not significant in the linear regime because of their relative strengths. If it is considered that $\chi^{(1)} = 1$, then the relative strengths of the higher order susceptibilities are typically of the order, $\chi^{(2)} \approx 10^{-10} \text{ cm/V}$ and $\chi^{(3)} \approx 10^{-17} \text{ cm}^2/\text{V}^2$. It is thus clear that only when the intensity of the incident light is sufficiently high, do the higher order polarization terms become significant. In general, all the susceptibilities are tensors. They take account of the polarization of the incident electric fields relative to the orientation of the medium, since generally the medium is anisotropic and hence responds differently for different polarization directions of the incident fields. It is, however, not necessary to consider them as tensors for this discussion, since their tensor character is not essential for this analysis.

The different orders of susceptibilities govern different processes that occur during light-matter interaction. The number of waves or photons that partake in an interaction determine

which $\chi^{(n)}$ describes the interaction. For instance, $\chi^{(1)}$ describes two-wave interactions, $\chi^{(2)}$ three-wave, $\chi^{(3)}$ four-wave and so forth. A three-wave interaction implies that two waves (with frequencies ω_1 and ω_2) enter the medium and one (with frequency ω_3) leaves, or one wave enters the medium and two leave the medium.

Energy, momentum and angular momentum must be conserved during these interactions. For the above example energy conservation implies that $\omega_3 = \omega_1 + \omega_2$ or $\omega_3 = \omega_1 - \omega_2$. In a degenerate case, $\omega_1 = \omega_2$, as is the case when only a single frequency laser is incident on the material. This implies that $\omega_3 = 2\omega_1$, and this is known as second harmonic generation. For a four-wave interaction, three waves are incident on the sample and one exits the sample. In this case $\chi^{(3)}$ describes the interaction. If all the incident waves have the same frequency, then the exiting wave can have a frequency three times the incident frequency (third harmonic generation) or equal to the incident frequency ($\omega_4 = \omega_1 - \omega_1 + \omega_1 = \omega_1$). Cases where the exiting wave and the incident wave are of the same frequency, but a nonlinear process has occurred, must therefore be described by at least the $\chi^{(3)}$ term, and cannot be described by a lower order term. An example of this is self focussing, which will be discussed in detail in Section 2.2.

To describe nonlinear light-matter interactions it is necessary to find a solution for Maxwell's equations (Equations 2.1 to 2.4), where the nonlinear polarization is now included. It is customary to separate the linear part from the nonlinear part by rewriting the polarization (Equation 2.16) in the form

$$\mathbf{P}(\mathbf{E}) = \epsilon_0(\epsilon_1 - 1)\mathbf{E} + \mathbf{P}_{\text{NL}} \quad (2.17)$$

with ϵ_1 the linear dielectric constant,

$$\begin{aligned} (\epsilon_1 - 1) &= \chi^{(1)} \\ \epsilon_1 &= \chi^{(1)} + 1 \end{aligned} \quad (2.18)$$

and \mathbf{P}_{NL} containing all the higher order polarization terms. In this form the electric displacement simply becomes

$$\mathbf{D}(\mathbf{E}) = \epsilon_0\epsilon_1\mathbf{E} + \mathbf{P}_{\text{NL}} \quad (2.19)$$

Maxwell's equations, including the nonlinear polarization term, can now be written as

$$\nabla \times \mathbf{H} = \frac{\partial}{\partial t} (\epsilon_0 \epsilon_1 \mathbf{E} + \mathbf{P}_{\text{NL}}) = \epsilon_0 \epsilon_1 \frac{\partial \mathbf{E}}{\partial t} + \frac{\partial \mathbf{P}_{\text{NL}}}{\partial t} \quad (2.20)$$

$$\nabla \times \mathbf{E} = -\frac{\partial}{\partial t} (\mu_0 \mathbf{H}) = -\mu_0 \frac{\partial \mathbf{H}}{\partial t} . \quad (2.21)$$

In order to solve this set of coupled differential equations, to extract the nonlinear wave equation, the rotation of Equation 2.21 is considered.

$$\begin{aligned} \nabla \times \nabla \times \mathbf{E} &= \nabla \times \left(-\mu_0 \frac{\partial \mathbf{H}}{\partial t} \right) \\ &= -\mu_0 \frac{\partial}{\partial t} (\nabla \times \mathbf{H}) . \end{aligned} \quad (2.22)$$

Substituting Equation 2.20 into Equation 2.22 yields

$$\nabla \times \nabla \times \mathbf{E} = -\mu_0 \frac{\partial}{\partial t} \left(\epsilon_0 \epsilon_1 \frac{\partial \mathbf{E}}{\partial t} + \frac{\partial \mathbf{P}_{\text{NL}}}{\partial t} \right) . \quad (2.23)$$

Using the general identity $\nabla \times (\nabla \times \mathbf{E}) = \nabla (\nabla \cdot \mathbf{E}) - \nabla^2 \mathbf{E}$ Equation 2.23 is rewritten as

$$\nabla (\nabla \cdot \mathbf{E}) - \nabla^2 \mathbf{E} = -\mu_0 \frac{\partial}{\partial t} \left(\epsilon_0 \epsilon_1 \frac{\partial \mathbf{E}}{\partial t} + \frac{\partial \mathbf{P}_{\text{NL}}}{\partial t} \right) \quad (2.24)$$

In general only transverse fields are considered, which implies that $\nabla \cdot \mathbf{E} = 0$. This simplifies Equation 2.24 as follows,

$$\begin{aligned} \nabla^2 \mathbf{E} &= \mu_0 \frac{\partial}{\partial t} \left(\epsilon_0 \epsilon_1 \frac{\partial \mathbf{E}}{\partial t} + \frac{\partial \mathbf{P}_{\text{NL}}}{\partial t} \right) \\ \nabla^2 \mathbf{E} &= \epsilon_0 \mu_0 \epsilon_1 \frac{\partial^2 \mathbf{E}}{\partial t^2} + \mu_0 \frac{\partial^2 \mathbf{P}_{\text{NL}}}{\partial t^2} \\ \nabla^2 \mathbf{E} &= \frac{\epsilon_1}{c^2} \frac{\partial^2 \mathbf{E}}{\partial t^2} + \frac{1}{c^2 \epsilon_0} \frac{\partial^2 \mathbf{P}_{\text{NL}}}{\partial t^2} \\ \nabla^2 \mathbf{E} - \frac{\epsilon_1}{c^2} \frac{\partial^2 \mathbf{E}}{\partial t^2} &= \frac{1}{c^2 \epsilon_0} \frac{\partial^2 \mathbf{P}_{\text{NL}}}{\partial t^2} , \end{aligned} \quad (2.25)$$

where the fact that $\epsilon_0 \mu_0 = c^{-2}$, with c being the speed of light in vacuum, is used. Equation 2.25 is known as the nonlinear inhomogeneous wave equation [3]. To obtain a solution of the nonlinear wave equation, it is assumed that the solution consists of a linear summation of plane

waves with discrete frequency components. The frequencies of these plane waves are ω_j and the accompanying wave vectors are $k_j = \frac{n^{(j)}\omega_j}{c}$. If it is further assumed that the plane waves only propagate along the z -axis, then the solutions can be described by [2]

$$\mathbf{E}(z, t) = \frac{1}{2} \left(\sum_{j=1}^N \mathbf{E}_j(z, t) e^{i(k_j z - \omega_j t)} + c.c. \right) \quad (2.26)$$

where *c.c.* refers to the complex conjugate of the first term and describes the waves travelling in the negative direction. In a completely analogous fashion [2] the nonlinear polarization can be written as

$$\mathbf{P}(z, t) = \frac{1}{2} \left(\sum_{j=1}^N \mathbf{P}_j(z, t) e^{-i\omega_j t} + c.c. \right) . \quad (2.27)$$

Since the complex conjugate terms only describe waves travelling in the negative direction, they do not yield any additional information. They are therefore discarded in the rest of the discussion. Taking the second order spatial derivative of the electric field and the second order temporal derivative of both the electric field and nonlinear polarization yields

$$\frac{\partial^2}{\partial z^2} \mathbf{E}(z, t) = \frac{1}{2} \sum_{j=1}^N \left(\frac{\partial^2 \mathbf{E}_j}{\partial z^2} + 2ik_j \frac{\partial \mathbf{E}_j}{\partial z} - k_j^2 \mathbf{E}_j \right) e^{ik_j z} e^{-i\omega_j t} \quad (2.28)$$

$$\frac{\partial^2}{\partial t^2} \mathbf{E}(z, t) = \frac{1}{2} \sum_{j=1}^N \left(\frac{\partial^2 \mathbf{E}_j}{\partial t^2} - 2i\omega_j \frac{\partial \mathbf{E}_j}{\partial t} - \omega_j^2 \mathbf{E}_j \right) e^{ik_j z} e^{-i\omega_j t} \quad (2.29)$$

$$\frac{\partial^2}{\partial t^2} \mathbf{P}_{\text{NL}}(z, t) = \frac{1}{2} \sum_{j=1}^N \left(\frac{\partial^2 \mathbf{P}_{\text{NL}j}}{\partial t^2} - 2i\omega_j \frac{\partial \mathbf{P}_{\text{NL}j}}{\partial t} - \omega_j^2 \mathbf{P}_{\text{NL}j} \right) e^{-i\omega_j t} . \quad (2.30)$$

Considering the electric field and the induced nonlinear polarization field, and assuming that spatially and temporally the amplitude changes very slowly, at least compared to the frequency of the plane wave, the following assumption can be made:

$$\frac{\partial^2 \mathbf{E}_j}{\partial t^2} \ll \omega_j \frac{\partial \mathbf{E}_j}{\partial t} \ll \omega_j^2 \mathbf{E}_j \quad (2.31)$$

$$\frac{\partial^2 \mathbf{E}_j}{\partial z^2} \ll k_j \frac{\partial \mathbf{E}_j}{\partial z} \ll k_j^2 \mathbf{E}_j \quad (2.32)$$

$$\frac{\partial^2 \mathbf{P}_{\text{NL}j}}{\partial t^2} \ll \omega_j \frac{\partial \mathbf{P}_{\text{NL}j}}{\partial t} \ll \omega_j^2 \mathbf{P}_{\text{NL}j} . \quad (2.33)$$

This assumption is known as the "slowly varying envelope approximation" (SVEA) [1]. The validity of the SVEA for the nonlinear polarization can be seen when considering the relative time scales. Light in the visible spectrum has a frequency of approximately $\omega_j \approx 10^{15}$ Hz. The time it takes to polarize the medium is roughly $t_p \geq 10^{-12}$ s. This has the result that the second order spatial and temporal derivatives of the amplitude of the electric field and the first and second order temporal derivative of the nonlinear polarization can be neglected under the SVEA. Combining the nonlinear inhomogeneous wave equation (Equation 2.25) with Equations 2.28, 2.29 and 2.30, and taking these omissions into account, yields

$$\begin{aligned} & \frac{1}{2} \sum_{j=1}^N \left(2ik_j \frac{\partial \mathbf{E}_j}{\partial z} - k_j^2 \mathbf{E}_j - \frac{\epsilon_j}{c^2} \left[-2i\omega_j \frac{\partial \mathbf{E}_j}{\partial t} - \omega_j^2 \mathbf{E}_j \right] \right) e^{i(k_j z - \omega_j t)} \\ &= \frac{1}{2} \frac{1}{c^2 \epsilon_0} \sum_{j=1}^N \left(-\omega_j^2 \mathbf{P}_{\text{NL}_j} \right) e^{-i\omega_j t} \end{aligned} \quad (2.34)$$

which can be further simplified by noting that $k_j^2 = \frac{\epsilon_j \omega_j^2}{c^2}$. This yields

$$\sum_{j=1}^N \left(2ik_j \frac{\partial \mathbf{E}_j}{\partial z} + 2i \frac{\epsilon_j}{c^2} \omega_j \frac{\partial \mathbf{E}_j}{\partial t} \right) e^{ik_j z} = \frac{-1}{c^2 \epsilon_0} \sum_{j=1}^N \omega_j^2 \mathbf{P}_{\text{NL}_j} . \quad (2.35)$$

This holds true for each of the frequency components and thus, keeping in mind that $n_j = \sqrt{\epsilon_j}$ and $k_j = \frac{n_j \omega_j}{c}$, it follows that

$$\frac{\partial \mathbf{E}_j}{\partial z} + \frac{n_j}{c} \frac{\partial \mathbf{E}_j}{\partial t} = i \frac{\omega_j}{cn_j} \frac{1}{2\epsilon_0} \mathbf{P}_{\text{NL}_j} e^{ik_j z} . \quad (2.36)$$

Equation 2.36 is then the well known, so-called nonlinear wave equation. It provides a framework for describing all the nonlinear light matter interactions. Two such interactions, self focussing and nonlinear absorption, will be described in some detail.

2.2 Self focusing (nonlinear refraction)

Self focusing is a nonlinear process. Since it is the fundamental laser beam that is influenced, it cannot be a three-wave interaction, but must be at least a four-wave interaction, as was shown in Section 2.1. In this analysis only a four-wave interaction will be considered since it

is the dominant interaction in the case of self focusing [1]. This implies that the $\chi^{(2)}$ term in Equation 2.16 will play no part during self focusing and can thus be neglected. Equation 2.16 will now read as follows

$$\mathbf{P}(\mathbf{E}) = \epsilon_0(\chi^{(1)}\mathbf{E} + \chi^{(3)}\mathbf{E}\mathbf{E}\mathbf{E} + \dots) \quad (2.37)$$

which can be rewritten as

$$\mathbf{P}(\mathbf{E}) = \frac{\epsilon_0}{2}(\chi^{(1)} + \chi^{(3)}|\mathbf{E}|^2 + \dots)\mathbf{E} . \quad (2.38)$$

Considering the bracket term to be the field-dependent susceptibility and disregarding the $\chi^{(4)}$ and higher terms, then analogously to the case of linear polarization (Equation 2.5), the nonlinear polarization can be written as

$$\mathbf{P}(\mathbf{E}) = \frac{\epsilon_0}{2}\chi(|\mathbf{E}|^2)\mathbf{E} \quad (2.39)$$

with

$$\chi(|\mathbf{E}|^2) = \chi^{(1)} + \chi^{(3)}|\mathbf{E}|^2 . \quad (2.40)$$

It was shown (Equation 2.18) that $\epsilon_1 = \chi^{(1)} + 1$. It is known [1] that the linear index of refraction, n_0 , relates to the dielectric constant through

$$n_0 = \sqrt{\epsilon_1} \quad (2.41)$$

for the case of negligible absorption, which implies that

$$n_0^2 = \chi^{(1)} + 1 . \quad (2.42)$$

This implies that the refractive index, n , can analogously be written as

$$n^2 = 1 + \chi(|\mathbf{E}|^2) \quad (2.43)$$

and thus

$$n = \left(1 + \chi^{(1)} + \chi^{(3)}|\mathbf{E}|^2\right)^{\frac{1}{2}} . \quad (2.44)$$

Using Equation 2.42 yields

$$\begin{aligned}
 n &= \left(n_0^2 + \chi^{(3)} |\mathbf{E}|^2 \right)^{\frac{1}{2}} \\
 &= n_0 \left(1 + \frac{\chi^{(3)} |\mathbf{E}|^2}{n_0^2} \right)^{\frac{1}{2}} \\
 &\approx n_0 + \frac{\chi^{(3)} |\mathbf{E}|^2}{2n_0^2} \equiv n_0 + \frac{n_2}{2} |\mathbf{E}|^2
 \end{aligned} \tag{2.45}$$

and hence

$$n = n_0 + n_2 \langle \mathbf{E} \cdot \mathbf{E} \rangle = n_0 + \Delta n \tag{2.46}$$

with n_2 being the nonlinear index of refraction

Self focusing can be easily understood, keeping in mind Equation 2.46, where it is shown that the refractive index is a function of the square of the electric field. This implies that the change in the refractive index, Δn , is a function of the intensity, $I(r)$.

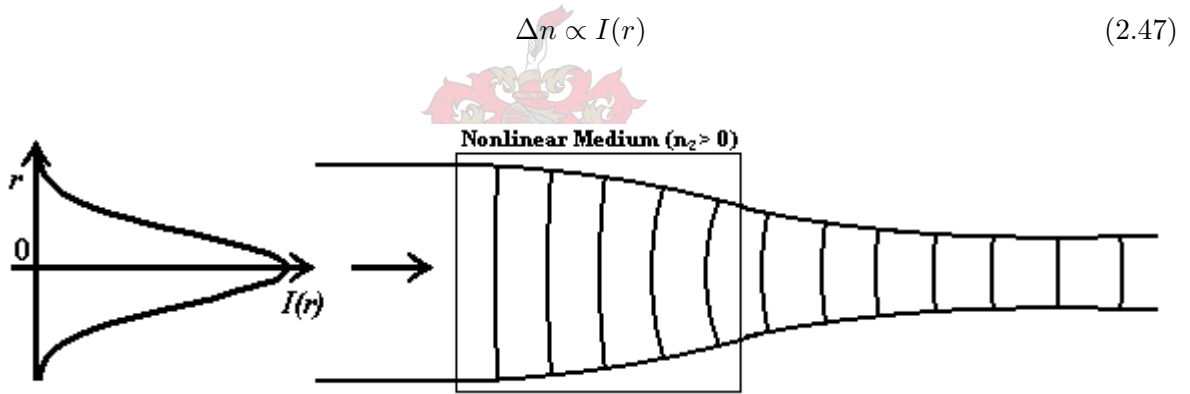


Figure 2-2: Self focusing of a Gaussian beam.

Considering incident laser light with a Gaussian intensity distribution, the intensity in the nonlinear material is higher in the centre of the pulse than in the flanks of the pulse. The result is that the change in the refractive index of the material will be greater in the centre of the pulse than in the flanks, which results in a greater phase change, $\Delta\phi(\Delta n)$, of the laser pulse in the centre than in the flanks. The result is that the material will act as a lens. This effect is illustrated in Figure 2-2. The sign of the nonlinear index of refraction will determine whether

focusing ($n_2 > 0$) or defocusing ($n_2 < 0$) will occur. Usually one distinguishes between weak self focusing and catastrophic self focusing, the difference being that in the first case the focus is outside the medium and in the second case it is within the medium.

2.2.1 Conditions for self focusing

To obtain an understanding of the conditions required for self focusing to occur, a summary of the discussion presented by Milonni and Eberly in their book "Lasers" [1] will be presented here. The wave equation for the electric field ($\mathbf{E} = E_0 e^{-i\omega t}$), with the index of refraction given by Equation 2.46, is considered

$$\nabla^2 \mathbf{E} - \frac{n^2}{c^2} \frac{\partial^2 \mathbf{E}}{\partial t^2} \approx \nabla^2 \mathbf{E} - \frac{1}{c^2} \left(n_0^2 + 2n_0 n_2 \mathbf{E}^2 \right) \frac{\partial^2 \mathbf{E}}{\partial t^2} = 0 \quad (2.48)$$

with the approximation that $n_2 \ll n_0$. In the paraxial approximation [1] and averaging over an optical period (which results in replacing \mathbf{E}^2 by $\frac{1}{2} |E_0|^2$) the result is

$$\nabla_T^2 E_0 + 2ik \frac{\partial E_0}{\partial z} + \frac{k^2 n_2}{n_0} |E_0|^2 E_0 = 0 \quad (2.49)$$

where $k = n_0 \omega / c$ and $\nabla_T^2 = \frac{\partial^2}{\partial x^2} + \frac{\partial^2}{\partial y^2}$ is the transverse Laplacian. The $\nabla_T^2 E_0$ describes how the beam changes perpendicular to the propagation direction and thus the beam spreading (diffraction) that occurs. Since it describes how the beam changes perpendicular to the propagation direction, it is dependent on the beam size or rather the beam cross section. In other words, beam spreading can be considered to be dependent on the beam cross section [1]. If the cross section is characterized by radius a_0 , then

$$\nabla_T^2 E_0 \sim a_0^{-2} E_0 \quad (2.50)$$

The $\frac{k^2 n_2}{n_0} |E_0|^2 E_0$ term is the intensity dependent part which describes the self focusing. Self focusing can compete with diffraction if $\frac{k^2 n_2}{n_0} |E_0|^2 E_0$ is comparable to $\nabla_T^2 E_0$, that is if

$$\frac{k^2 n_2}{n_0} |E_0|^2 E_0 \sim a_0^{-2} E_0 \quad (2.51)$$

or

$$a_0^2 |E_0|^2 \sim \frac{n_0}{k^2 n_2} . \quad (2.52)$$

The beam intensity, I , is related to the square of the electric field through $I = (n_0 c \epsilon_0 / 2) |E_0|^2$. The power, P , is related to the product of the intensity and the cross section of the beam. Using Equation 2.52 the critical beam power that is necessary to overcome the diffractive spreading of the beam is of the order

$$\begin{aligned} P_{\text{cr}} \sim (\pi a_0^2) I &= \frac{\pi n_0 c \epsilon_0}{2} a_0^2 |E_0|^2 \\ &= \frac{\pi n_0 c \epsilon_0}{2} \frac{n_0}{k^2 n_2} \\ &= \frac{\pi n_0^2 c \epsilon_0}{2 k^2 n_2} \\ &= \frac{c \epsilon_0 \lambda^2}{8 \pi n_2} . \end{aligned} \quad (2.53)$$

This approximation is in good agreement [1] with numerical integration of the nonlinear partial differential Equation 2.49. It can be seen that it is the beam power that must exceed a certain threshold for self focusing and not the beam intensity. A beam with power less than P_{cr} will not undergo self focusing even if it is focussed tighter [1]. The reason for this is that the diffractive spreading increases as the beam diameter is reduced, counteracting the self focusing.

2.3 Nonlinear absorption

When considering absorption, the well known Beer's law is applicable to linear absorption

$$I(z) = I_0 e^{-\alpha(\omega)z} \quad (2.54)$$

where I_0 is the incident intensity, $\alpha(\omega)$ is the linear absorption coefficient, z is the propagation depth in the absorbing medium and $I(z)$ is the intensity at depth z . Beer's law is merely the solution of the differential equation that describes how light intensity decreases with propagation depth in a medium for the case where α is a constant,

$$\frac{\partial I}{\partial z} = -\alpha(\omega)I . \quad (2.55)$$

If nonlinear (multi-photon) effects are to be included then this differential equation must be extended to include higher order intensity terms [4],

$$\frac{\partial I}{\partial z} = -\alpha(\omega)I - \beta(\omega)I^2 - \gamma(\omega)I^3 - O(I^4) \quad (2.56)$$

where $\beta(\omega)$ is the two-photon absorption coefficient, $\gamma(\omega)$ is the three-photon absorption coefficient and $O(I^4)$ represents the four-photon and higher absorption terms.

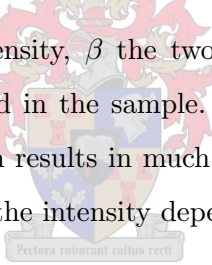
If a material displays negligible linear absorption and two-photon absorption dominates, then only the second term on the right of Equation 2.56 needs to be considered and the other terms can be disregarded. This implies that only

$$\frac{\partial I}{\partial z} = -\beta(\omega)I^2 \quad (2.57)$$

needs to be solved. This can be done by separation of variables [4] which yields

$$I(z) = \frac{I_0}{1 + \beta I_0 z} \quad (2.58)$$

where I_0 is again the incident intensity, β the two-photon absorption coefficient and z the distance that the light has travelled in the sample. It can clearly be seen from Figures 2-3 and 2-4 that two-photon absorption results in much stronger absorption and thus more beam attenuation. This is as a result of the intensity dependent nature of nonlinear absorption.



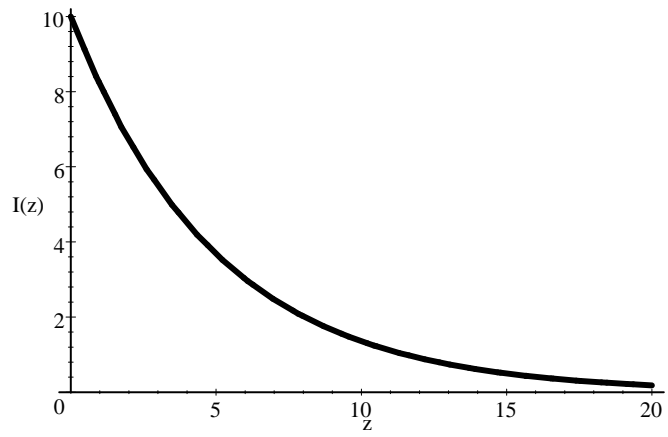


Figure 2-3: A schematic graph depicting linear absorption, z being the depth in the sample ($I_0 = 10$, $\alpha = 0.2$).

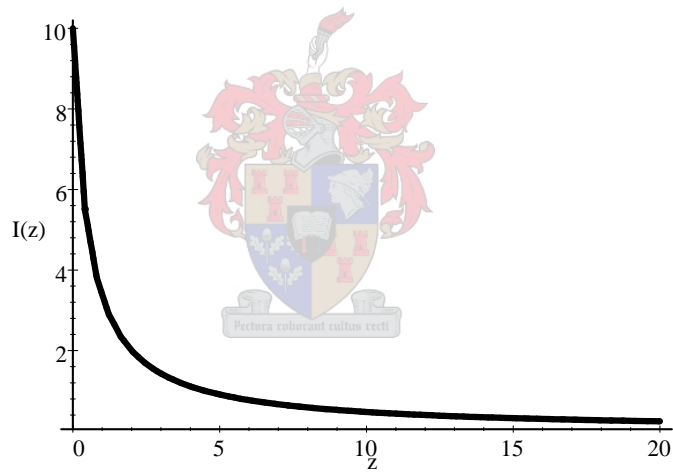


Figure 2-4: A schematic graph depicting pure two-photon absorption, z being the depth in the sample ($I_0 = 10$, $\beta = 0.2$).

Chapter 3

The Z-scan as analysis technique

There are numerous techniques for measuring the nonlinear index of refraction and the nonlinear absorption coefficient of materials. The Z-scan is amongst the simplest and most sensitive of these techniques. The basic Z-scan technique has been described by Mansoor Sheik-Bahae *et al* [5][6] and a brief summary of the theory of the technique is presented here. The most important aspects to be considered for an experimental setup, along with some of the constraints that need to be placed on the design of the setup, will be highlighted.

3.1 The Z-scan

The Z-scan works on the principle of moving the sample under investigation through the focus of a tightly focussed Gaussian laser beam. The interaction of the medium with the laser light changes as the sample is moved. This is because the sample experiences different intensities, dependent on the sample position (z) relative to the focus ($z = 0$). By measuring the transmitted power (the transmittance) through the sample as a function of z -position of the sample, information about the light-matter interaction can be extracted. The two nonlinear interactions that can be determined in this fashion are the sample's nonlinear index of refraction and nonlinear absorption coefficient. For the measurement of the nonlinear index of refraction an aperture is placed in front of the detector measuring the transmitted light. This makes the measurement sensitive to beam spreading or focusing and relates to a transformation of phase distortion into amplitude distortion. The basic setup can be seen in Figure 3-1. In the figure,

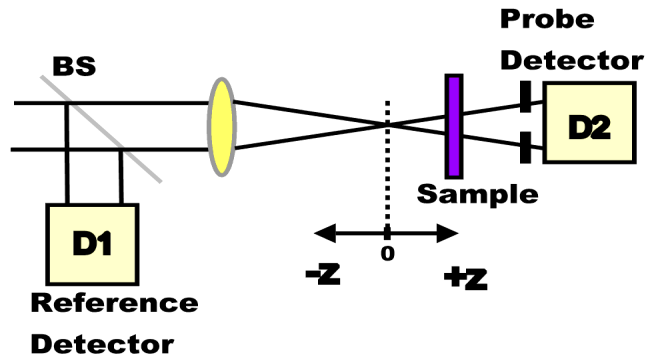


Figure 3-1: The basic Z-scan setup.

BS is a beamsplitter, D1 is the reference detector, D2 the probe detector and the sample is at position z . An aperture is placed in front of the probe detector when measuring the nonlinear index of refraction.

A sample displaying nonlinear refraction will act as a lens of variable focal length as it is moved along the z -axis. An example of this is the following: Consider a material with a negative nonlinear index of refraction and a thickness less than the diffraction length (also known as the Rayleigh length, z_0) of the focussed laser beam. (The reason for this limitation is explained in Section 3.2.) The sample exhibits negligible nonlinear refraction when it is far from the focus, because of the low intensity of the laser beam at this position. As the sample is moved towards the focus it starts acting as a negative lens, collimating the beam and shifting the waist of the laser beam. The result is a smaller spot size at the aperture placed in front of the detector, and thus a higher transmittance through the aperture (see Figure 3-2). This effect increases as the sample is moved towards the focus due to the intensity increase. A maximum transmittance through the aperture will occur when the sample is just in front of the focus. This maximum in transmittance (peak) will drop to a minimum (valley) as the sample is moved further and the beam diverges as a result of the negative lensing by the sample. The transmittance through the aperture will again return to the linear value as the sample is moved further from the focus. The result of a scan such as this is a transmittance versus position

graph which has a peak followed by a valley. When the sample has a positive nonlinear index of refraction, the graph is inverted. This is illustrated in Figure 3-3.

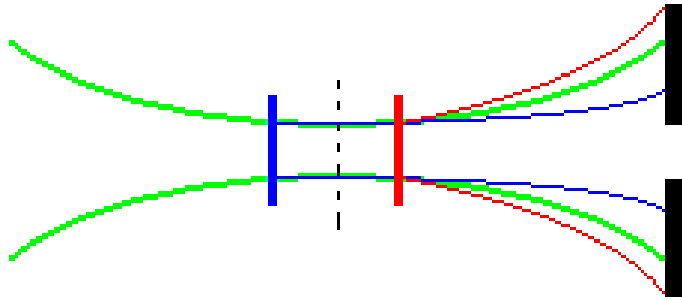


Figure 3-2: Illustration of the influence on the spot size of a Gaussian beam as a result of an interaction with a sample having a negative nonlinear index of refraction. (green = unattenuated beam, blue = sample before focus, red = sample after focus)

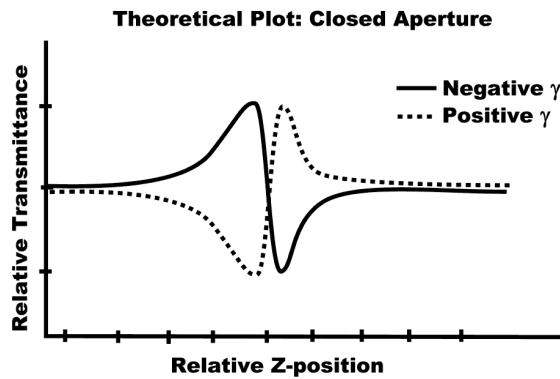


Figure 3-3: Traces showing the transmittance through a sample with a positive or a negative nonlinear index of refraction (γ).

The sign of the nonlinear index of refraction of a sample is thus immediately clear from the shape of the graph. It is important to note that in most cases nonlinear refraction does not occur on its own, but usually in conjunction with nonlinear absorption. This implies that the

data from a Z-scan will contain both nonlinear refraction and nonlinear absorption. To extract the nonlinear index of refraction it is necessary to perform a Z-scan with the aperture removed, in order to measure the total transmittance of the sample. The measured transmittance is then independent of nonlinear refraction and only dependent on nonlinear absorption. It will be shown in the following paragraphs that the data from such a Z-scan with the aperture removed, when plotted, forms a valley that is symmetric around the focus (see Figure 3-4). This open aperture Z-scan is used to determine the nonlinear absorption coefficient. The nonlinear index of refraction can be obtained by dividing the data obtained from the Z-scan with the aperture in place by the data obtained from the open aperture Z-scan. The data from these two scans as well as the result of dividing the two sets of data by each other can be seen in Figure 3-4.

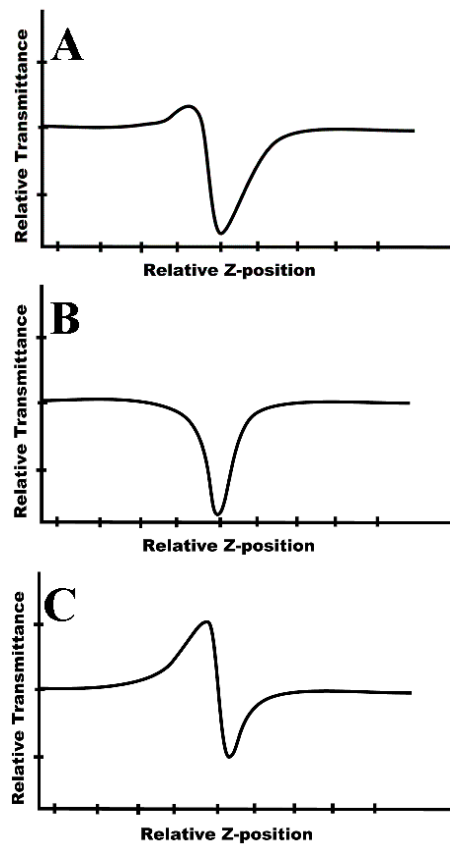


Figure 3-4: A) A closed aperture Z-scan, B) an open aperture Z-scan and C) the result of dividing the closed aperture Z-scan by the open aperture Z-scan.

3.2 Theory

The theory of the Z-scan was developed by Mansoor Sheik-Bahae *et al* [5][6]. The following sections on nonlinear refraction and nonlinear absorption are adapted from the existing theory. Any assumptions and simplifications are taken from this theory.

3.2.1 Nonlinear refraction

The general theory on which the Z-scan is based is merely a specific case of the theory of the nonlinear light-matter interaction discussed in Chapter 2. For the analysis of the Z-scan, a TEM₀₀ Gaussian beam, with associated electric field, $E(r, t, z)$, will be considered interacting with the sample. The procedure followed in deriving the relevant equations describing the data obtained from a Z-scan can be explained by the following steps (see also Figure 3-5): (i) The properties of the Gaussian beam, $E(r, t, z)$, will be described at the sample position, z , relative to the focus ($z = 0$). (ii) The sample introduces a phase shift, $\Delta\phi(r, t, z, L)$, due to nonlinear refraction. The properties of the Gaussian beam exiting the sample, $E_e(r, t, z)$, will then be described. (iii) This Gaussian beam will then be allowed to propagate a distance d through free space up to the aperture plane where, again, its properties ($E_a(r, t, z)$) will be described. (iv) Lastly, the transmittance through the aperture, $T(z)$, will be calculated.

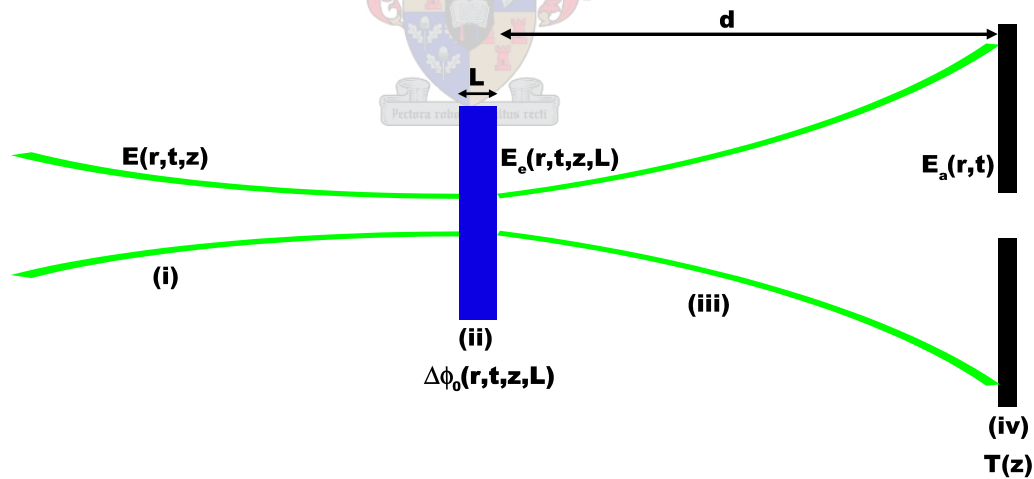


Figure 3-5: A schematic representation of the Gaussian beam's interaction with the sample. The lettering and numbering correspond to those in the text.

(i) Gaussian beam at the sample

The electric field, $E(r, t, z)$, of a Gaussian beam with a waist radius w_0 , propagating in the $+z$ direction at a distance z from the waist, can be written as

$$E(r, t, z) = E_0(t) \frac{w_0}{w(z)} \cdot \exp\left(-\frac{r^2}{w^2(z)} - \frac{ikr^2}{2R(z)}\right) e^{-i\phi(z,t)} \quad (3.1)$$

where the beam radius $w(z)$ is related to the z -position through $w^2(z) = w_0^2 \left(1 + \frac{z^2}{z_0^2}\right)$, the radius of curvature of the wavefront at z is given by $R(z) = z \left(1 + \frac{z_0^2}{z^2}\right)$, $z_0 = kw_0^2/2$ is known as the Rayleigh length or diffraction length of the beam, $k = 2\pi/\lambda$ is the wave vector, and λ is the laser wavelength, all in free space. $E_0(t)$ contains the temporal envelope of the laser pulse and denotes the radiation electric field at the waist.

The phase variations that are independent of r are contained in the $e^{-i\phi(z,t)}$ term. For the following discussion, only the radial phase variations, $\Delta\phi(r)$, are of interest and hence all the phase changes that are uniform in r are not considered in the discussion. Hence the $e^{-i\phi(z,t)}$ term is omitted in the subsequent analysis.

(ii) Introducing the phase shift

As was mentioned earlier, in the analysis of the Z-scan it is necessary to consider the index of refraction of the sample to not only include the linear index of refraction, but to also be dependent on the nonlinear indexes of refraction, n_2 (esu) or γ (m^2/W), through

$$n = n_0 + \frac{n_2}{2} |E|^2 = n_0 + \gamma I = n_0 + \Delta n \quad (3.2)$$

where n_0 is the linear index of refraction, E is the electric field (cgs) and I is the intensity (MKS) of the laser beam within the sample (n_2 and γ are related through $n_2(\text{esu}) = \frac{c n_0}{40\pi} \gamma(\text{m}^2/\text{W})$).

For the analysis it is necessary that the sample be considered "thin" [5]. The sample under investigation can be considered as such if the sample length (L) is small enough that changes in beam diameter within the sample, due either to diffraction or nonlinear refraction, can be ignored. This allows one to consider the interaction between the laser pulse and the sample to happen at only one position, and not to be spread out over the entire interaction length. In

this case the self refraction is called "external self-action" [5]. For diffraction this implies that $L \ll z_0$, while for nonlinear refraction $L \ll z_0/\Delta\phi(0)$ [5]. In most Z-scan experiments the second criterion has been found to be automatically met since $\Delta\phi(0)$ is usually small [5]. It has been found experimentally that the first criterion placed on the linear diffraction is more restrictive than it needs to be and that $L < z_0$ is sufficient [5]. This assumption simplifies the problem and if the interaction is now considered in the SVEA, which was discussed in Section 2.1, the following differential equations hold true:

$$\frac{d\Delta\phi(r, t, z, L)}{dz'} = \Delta n(I) k \quad (3.3)$$

and

$$\frac{dI}{dz'} = -\alpha(I) I \quad (3.4)$$

with z' the propagation depth in the sample and where $\alpha(I)$ includes both the linear and nonlinear absorption terms. These equations govern the Gaussian beam propagation through the sample, since the propagation of a Gaussian beam is described by its phase and amplitude. Equations 3.3 and 3.4 can be solved [5], when negligible nonlinear absorption and only a cubic nonlinearity is considered, to yield the phase shift $\Delta\phi$ at the exit surface of the sample, namely

$$\Delta\phi(r, t, z, L) = \Delta\phi_0(t, z, L) \exp\left(-\frac{2r^2}{w^2(z)}\right) \quad (3.5)$$

with

$$\Delta\phi_0(t, z, L) = \frac{\Delta\Phi_0(t, L)}{1 + \frac{z^2}{z_0^2}} \quad (3.6)$$

and $\Phi_0(t)$, the on-axis phase shift at the waist, defined as

$$\Delta\Phi_0(t, L) = k\Delta n(t)L_{\text{eff}} \quad , \quad (3.7)$$

where $L_{\text{eff}} = \frac{1-e^{-\alpha L}}{\alpha}$ with L the sample length, and α the linear absorption coefficient. Here $\Delta n(t) = \gamma I_0(t)$ with $I_0(t)$ the on-axis intensity at the focus ($z = 0$) in the sample since Fresnel reflection losses have been ignored. If the phase shift that the sample created is now included

in the equation, describing the Gaussian beam,

$$E_e(r, t, z, L) = E(r, t, z) e^{-\alpha L/2} e^{i\Delta\phi(r,t,z,L)} \quad (3.8)$$

is obtained. Since the dependence on L is inherent in the specific setup, the dependence will be omitted in the rest of the discussion:

$$E_e(r, t, z) = E_e(r, t, z, L) . \quad (3.9)$$

(iii) Propagation of Gaussian beam through free space

By using the complex electric field exiting the sample,

$$E_e(r, t, z) = E(r, t, z) e^{-\alpha L/2} e^{i\Delta\phi(r,t,z)} , \quad (3.10)$$

it is possible to obtain the far-field pattern of the beam at the aperture plane using the Huygens principle, by performing a zeroth-order Hankel transformation of E_e . This is a complicated mathematical procedure and a much simpler approach, namely Gaussian Decomposition (GD), as given by Weaire *et al* [7] and implemented by Sheik-Bahae *et al* [5], will be followed here. In this approach the complex electric field at the exit plane of the sample is decomposed into a summation of Gaussian beams through a Taylor series expansion of the nonlinear phase term. The reason for this approach is that generally only small phase changes are considered, which implies that only the first few terms of the Taylor expansion need to be considered.

$$e^{i\Delta\phi(z,r,t)} = \sum_{m=0}^{\infty} \frac{[i\Delta\phi_0(z, t)]^m}{m!} e^{-2mr^2/w^2(z)} \quad (3.11)$$

In this approach each Gaussian beam is propagated individually to the aperture plane where they are resummed to reconstruct the beam. The resultant field pattern at the aperture (E_a), taking the initial beam curvature for the focused beam into account, can be derived [5] as

$$E_a(r, t) = E(z, r = 0, t) e^{-\alpha L/2} \sum_{m=0}^{\infty} \frac{[i\Delta\phi_0(z, t)]^m}{m!} \frac{w_{m0}}{w_m} \cdot \exp\left(-\frac{r^2}{w_m^2} - \frac{ikr^2}{2R_m} + i\theta_m\right) . \quad (3.12)$$

If we consider d to be the propagation distance in free space from the sample to the aperture plane and $g = 1 + d/R(z)$, $R(z)$ being the radius of curvature, then the remaining parameters in 3.12 can be expressed as

$$w_{m0}^2 = \frac{w^2(z)}{2m+1} \quad (3.13)$$

$$w_m^2 = w_{m0}^2 \left[g^2 + \frac{d^2}{d_m^2} \right] \quad (3.14)$$

$$R_m = d \left[1 - \frac{g}{g^2 + d^2/d_m^2} \right]^{-1} \quad (3.15)$$

$$\theta_m = \tan^{-1} \left[\frac{d/d_m}{g} \right] \quad (3.16)$$

$$d_m = \frac{kw_{m0}^2}{2} . \quad (3.17)$$

(iv) Transmittance through the aperture

The transmitted power $P_T(\Delta\Phi_0(t))$ through the aperture is obtained by spatially integrating 3.12 up to the aperture radius r_a , which yields [5]

$$P_T(\Delta\Phi_0(t)) = c\epsilon_0 n_0 \pi \int_0^{r_a} |E_{a(r,t)}|^2 r dr \quad (3.18)$$

with ϵ_0 the permittivity of vacuum. Including the temporal variation of the pulse, the normalised Z-scan transmittance can be calculated as

$$T(z) = \frac{\int_{-\infty}^{\infty} P_T(\Delta\Phi_0(t)) dt}{S \int_{-\infty}^{\infty} P_i(t) dt} \quad (3.19)$$

where $P_i(t) = \pi w_0^2 I_0(t)/2$ is the instantaneous input power (within the sample), $S = 1 - \exp(-2r_a^2/w_a^2)$ is the linear transmittance through the aperture and w_a is the beam radius of the beam at the aperture.

For further analysis a steady state result is considered which implies an instantaneous non-linearity and a temporally square pulse. This is equivalent to considering CW radiation. This will later be expanded to include pulsed radiation. It is important to note that for a given $\Delta\Phi_0$, the magnitude and shape of $T(z)$ does not depend on the geometry or the wavelength, as long as the far-field condition for the aperture plane, namely $d \gg z_0$, is satisfied. An important

parameter in the Z-scan is the aperture size S , since a large aperture reduces the variations in $T(z)$. For a very large or no aperture ($S = 1$), these variations disappear altogether and $T(z) = 1$, independent of the z -position or $\Delta\Phi_0$.

For analysis purposes matters are simplified by defining an easily measurable quantity ΔT_{p-v} (see Figure 3-6) as the difference between the normalised peak and valley transmittance. The variation of this quantity as a function of $|\Delta\Phi_0|$ can be calculated and it can be shown that this dependence is almost linear for a specific aperture size. Furthermore, this value is independent of the geometry or laser wavelength. This dependence can be described [5], to within a $\pm 2\%$ accuracy, to be

$$\Delta T_{p-v} \simeq 0.406(1 - S)^{0.25} |\Delta\Phi_0| \quad (3.20)$$

for

$$|\Delta\Phi_0| \leq \pi \quad (3.21)$$

Equation 3.20 allows us to readily determine the nonlinear index of refraction to within very good accuracy. One of the important things evident from this analysis is that the limitation on the accuracy of the nonlinear index of refraction is only determined by the experimental setup and the optical quality of the sample under investigation, since these usually introduce errors greater than 2%.

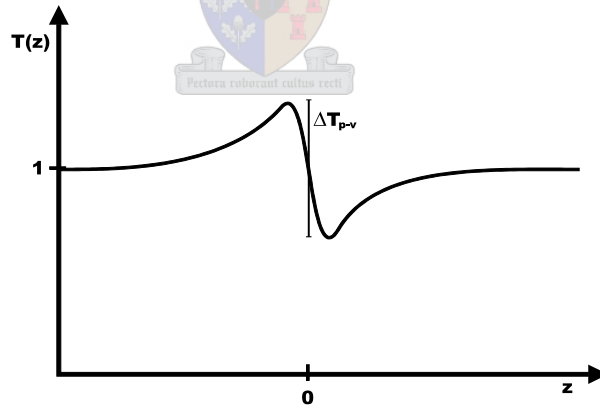


Figure 3-6: A graph illustrating the meaning of ΔT_{p-v} .

It is now possible to expand this analysis to include the transient effects induced by pulsed

radiation by merely using the time-averaged index of refraction change $\langle \Delta n(t) \rangle$ where

$$\langle \Delta n(t) \rangle = \frac{\int_{-\infty}^{\infty} \Delta n I_0(t) dt}{\int_{-\infty}^{\infty} I_0(t) dt} . \quad (3.22)$$

Considering a nonlinearity having an instantaneous response and decay time relative to the pulse width of the laser, for a temporally Gaussian pulse the following relation can be obtained,

$$\langle \Delta n(t) \rangle = \Delta n / \sqrt{2} \quad (3.23)$$

where Δn represents the peak-on-axis index change at the focus. $\langle \Delta \Phi_0(t) \rangle$ is related to $\langle \Delta n(t) \rangle$ through Equation 3.7.

All these equations were obtained by considering a third-order nonlinearity. It is possible to deal with higher-order nonlinearities in a similar fashion [6]. For higher nonlinearities one expects similar quantitative features from a Z-scan. Considering a fifth-order nonlinearity, $\chi^{(5)}$, which occurs in semiconductors where the index of refraction is influenced by charge carriers generated through two-photon absorption (a sequential $\chi^{(3)} : \chi^{(1)}$ effect), the nonlinear index of refraction change is only represented by $\Delta n = \eta I^2$. Following the same steps, a result similar to the one obtained for a third-order nonlinearity is obtained [5], namely

$$\Delta T_{p-v} \simeq 0.21(1 - S)^{0.25} |\Delta \Phi_0| . \quad (3.24)$$

3.2.2 Nonlinear absorption

As was mentioned earlier (Section 3.1), a Z-scan can also be used to determine the nonlinear absorption coefficient. For this measurement, the aperture is removed, making the scan insensitive to nonlinear refraction. It should be clear that the transmittance versus sample position graph of such an open aperture Z-scan should be symmetric around the focus since the intensity distribution of a Gaussian beam is symmetric around the focus. In the following analysis only two-photon absorption (2PA) is considered. This implies that it is still the third-order nonlinear susceptibility which governs the nonlinear absorption since the third-order nonlinear

susceptibility can be considered to be a complex quantity,

$$\chi^{(3)} = \chi_{\text{R}}^{(3)} + i\chi_{\text{I}}^{(3)} \quad , \quad (3.25)$$

with the imaginary part related to the 2PA coefficient, β , through

$$\chi_{\text{I}}^{(3)} = \frac{n_0^2 \epsilon_0 c^2}{\omega} \beta \quad , \quad (3.26)$$

ω being the optical frequency, and the real part is related to the nonlinear index of refraction, γ , through

$$\chi_{\text{R}}^{(3)} = 2n_0^2 \epsilon_0 c \gamma \quad . \quad (3.27)$$

In the preceding section where nonlinear refraction was considered, negligible nonlinear absorption was assumed. Now Equations 3.4 and 3.3, shown here again as Equations 3.29 and 3.30, must be re-examined with the following substitution taken into account

$$\alpha(I) = \alpha + \beta I \quad (3.28)$$

$$\frac{d\Delta\phi(r, t, z, L)}{dz'} = \Delta n(I) k \quad (3.29)$$

$$\frac{dI}{dz'} = -\alpha(I) I \quad . \quad (3.30)$$

The solutions of these differential equations [6] yield the irradiance distribution and phase shift of the laser beam at the exit surface of the sample as

$$I_e(z, r, t) = \frac{I(z, r, t) e^{-\alpha L}}{1 + q(z, r, t)} \quad (3.31)$$

$$\Delta\phi(z, r, t) = \frac{k\gamma}{\beta} \ln [1 + q(z, r, t)] \quad (3.32)$$

with $q(z, r, t) = \beta I L_{\text{eff}}$, where z is again the sample position with respect to the focus, β is the nonlinear absorption coefficient and L_{eff} is again the effective length of the sample, $L_{\text{eff}} = \frac{1 - e^{-\alpha L}}{\alpha}$, with α the linear absorption coefficient and L the actual length of the sample. By using Equations 3.31 and 3.32 the complex electric field at the exit surface of the sample

can be determined,

$$E_e = E(z, r, t)e^{-\alpha L/2} (1 + q)^{\left(\frac{ik\gamma}{\beta} - \frac{1}{2}\right)} . \quad (3.33)$$

Equation 3.33 reduces to Equation 3.10 in the limit where no two-photon absorption occurs. Generally [6], a zeroth order Hankel transform of Equation 3.33 will give the field distribution at the aperture, which can be used in Equations 3.18 and 3.19 to yield the transmittance. If only values of q such that $|q| < 1$ are considered, a binomial expansion of Equation 3.33 can be done in powers of q , resulting in an infinite sum of Gaussian beams, similar to what was done for the purely refractive case. This yields

$$E_e = E(z, r, t)e^{-\alpha L/2} \sum_{m=0}^{\infty} \frac{q(z, r, t)^m}{m!} \cdot \left[\prod_{n=0}^m (ik\gamma/\beta - 1/2 - n + 1) \right] \quad (3.34)$$

where the Gaussian spatial profiles are implicit in $q(z, r, t)$ and $E(z, r, t)$. The complex field pattern at the aperture plane can be obtained in the same manner as was previously done. The result can again be represented by 3.12 as long as the $(i\Delta\phi_0(z, t))^m/m!$ terms are substituted by

$$f_m = \frac{(i\Delta\phi_0(z, t))^m}{m!} \prod_{n=0}^m \left(1 + i(2n-1) \frac{\beta}{2k\gamma} \right) \quad (3.35)$$

with $f_0 = 1$. It should be noted that the coupling factor $\beta/2k\gamma$ is the ratio of the imaginary to real parts of the third-order nonlinear susceptibility, $\chi^{(3)}$.

The Z-scan transmittance variations can now be calculated in the same manner as was done previously. From Equation 3.35 it can be seen that absorptive and refractive contributions to the far-field beam profile, and thus to the Z-scan transmittance, are coupled. With the aperture removed the Z-scan transmittance is insensitive to nonlinear refraction and is thus only a function of the nonlinear absorption. It is thus sufficient to spatially integrate Equation 3.31 for the case of no aperture ($S = 1$), excluding the free-space propagation process.

Integrating Equation 3.31 at z over r , we obtain the transmitted power as

$$P(z, t) = P_i(t)e^{-\alpha L} \frac{\ln [1 + q_0(z, t)]}{q_0(z, t)} \quad (3.36)$$

with

$$q_0 = \frac{\beta I_0 L_{\text{eff}}}{1 + \frac{z^2}{z_0^2}} \quad (3.37)$$

and with $P_1(t)$ defined as it was in Equation 3.19. Assuming a Gaussian pulse, then Equation 3.36 can be time integrated to give the normalised energy transmittance as

$$T(z) = \frac{1}{\sqrt{\pi} q_0(z)} \int_{-\infty}^{\infty} \ln [1 + q_0(z) e^{-\tau^2}] d\tau \quad (3.38)$$

For $|q_0| < 1$ the transmittance function can be rewritten in a form more suitable to numerical analysis, namely

$$T(z) = \sum_{m=0}^{\infty} \frac{[-q_0(z)]^m}{(m+1)^{\frac{3}{2}}} \quad (3.39)$$

The nonlinear absorption coefficient, β , can be determined unambiguously by fitting this function to the transmittance data obtained from an open aperture Z-scan. Having found β , γ can be determined from the Z-scan with the aperture in place. This formulation, however, puts some restrictions on the experiment. The fact that $|q_0| < 1$ results in a limitation on the level of nonlinear absorption for which this numerical analysis is possible. This can be seen from Figure 3-7.

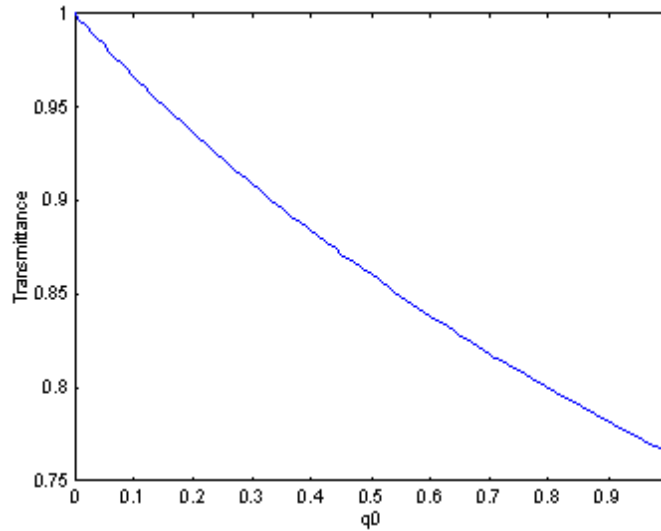


Figure 3-7: A graph depicting the lowest possible useful transmittance for numerical analysis.

If higher absorbancies need to be considered, it becomes necessary to fit the temporal integral, Equation 3.38, to the data. The advantage of using Equation 3.39 is that it is not necessary to compute a large number of terms in the sum as the series converges relatively quickly. This can be seen if one considers Figure 3-8, which depicts the value of $T(z)$ versus m for $q_0(z) = 0.99$. The fluctuations in $T(z)$ increase with larger q_0 and hence the choice of $q_0(z) = 0.99$.

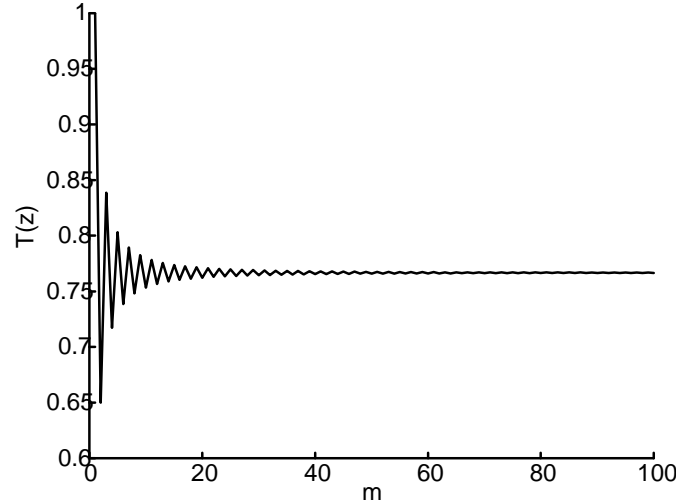


Figure 3-8: A schematic representation of how $T(z)$ varies with m , showing the quick convergence.

In conclusion, it is useful to notice that the assumptions that were made throughout this theory, translates into the assumption that the nonlinear absorption and nonlinear refraction occur completely independent of each other. This enables the extraction of the purely refractive Z-scan data from the closed aperture Z-scan, which contains the effects of both nonlinear absorption and nonlinear refraction, by dividing the data from the closed aperture Z-scan by the data from the open aperture Z-scan, as was explained at the end of Section 3.1.

Chapter 4

Experimental setup and considerations of the Z-scan technique

4.1 Refinement of experimental setup

A brief account is now given of how the basic Z-scan setup, as depicted in Figure 3-1, was expanded to become a useful laboratory facility with which practically any sample can be investigated.

Initial measurements were conducted using a very rough setup. This was done for the purpose of merely determining whether the nonlinear effects were clearly visible and easily measurable. The only component that remained the same in the final setup was the laser used, namely a pulsed Dye laser, the specifications of which is given in the Appendix. During these initial measurements an optical rail was used as translation stage and the sample was moved manually. This limited the accuracy and introduced alignment errors as a result of vibrational instability in the setup. The probe and reference energy were measured by two pyro-electric detectors. This limited the lower range of the energy that could be used as these detectors were not very sensitive in the microjoule range. Data acquisition was also performed manually, which was extremely laborious and time consuming. These measurements

did however prove that the setup worked in principle and that the nonlinear effects were clearly visible. These measurements highlighted the important areas to concentrate on and indicated what needed to be improved to enable more accurate measurements to be made. From these initial measurements the following systematic improvements were made:

(i) Detectors

The pyro-electric detectors were replaced by large area photodiodes (Thorlabs FDS1010). This vastly increased the sensitivity of the measurements. The photodiodes did, however, have a problem with saturation and care needed to be taken to avoid this. To this end, both detectors were shielded by neutral density filters.

(ii) Translation stage

The scanning of the sample was also improved by placing the sample on an automated translation stage. This improved the precision with which the sample could be moved and also eliminated some of the problems that were experienced with vibration and misalignment. The implementation of the automatic translation stage required the manufacturing of a stepper motor controller and the writing of control software.

(iii) Data acquisition

Lastly, the data acquisition was automated. This eliminated any user error and increased the speed of a scan. A data acquisition card (the details of which can be found in the Appendix) was installed and used to capture the data from the detectors. Customized software was developed and tested to handle the automated data acquisition. One of the factors that needed to be considered was that the large area photodiodes produced very fast (~ 40 ns) pulses, too fast for the data acquisition card to capture. This necessitated the use of extra electronic components to convert these pulses to signals that the data acquisition card could handle. For this purpose, two boxcar integrators (Stanford Research Systems SR250) were used to capture the peak values of the electrical pulses that the two photodiodes produced and to convert them to DC signals. The data acquisition card could easily sample DC signals.

Each of the abovementioned improvements increased the reproducibility of consecutive measurements and the reliability of the measurements. The systematic refinement was an iterative process, resulting in the final setup which can be seen in Figure 4-1. It is explained in Section 4.2.

4.2 Experimental setup

The basic Z-scan setup (Figure 3-1) was expanded to incorporate the improvements explained in Section 4.1. The expanded setup can be seen in Figure 4-1.

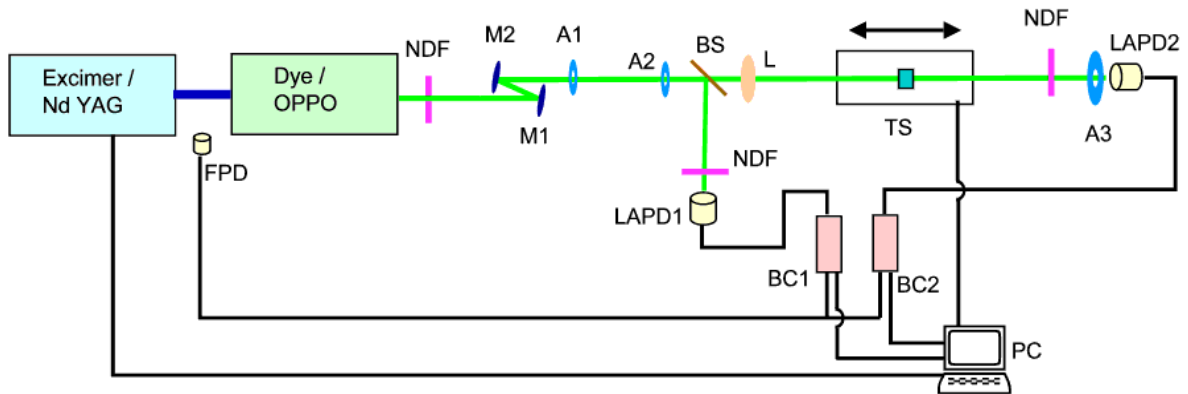


Figure 4-1: The final Z-scan setup used in the experiments.

The experimental setup can be explained as follows: An XeCl Excimer laser (Lambda Physik EMG 101 MSC) ($\lambda = 308$ nm) was used to pump a Dye laser (Lambda Physik FL3001) (λ tunable). The setup was designed to also be used with a frequency tripled Nd:YAG (Continuum Powerlite) ($\lambda = 355$ nm) pumped Optically Pumped Parametric Oscillator (OPPO) (Lambda Physik Scanmate OPPO) which provides easier tunability and thus greater versatility. The Dye laser beam was attenuated using different neutral density filters (NDF) to obtain the desired energy for the measurements. The beam then passed onto two mirrors (M1 and M2), used for laser alignment. Next the beam passed through two apertures (A1 and A2), used to improve the beam shape. (This will be expanded on in Section 4.3.1.) A beamsplitter (BS) was inserted into the beam to split the beam in two. The weaker part went to the reference detector, a large area photodiode (LAPD1), after passing through another neutral density filter (NDF), which

prevented the detector saturating. The main part of the beam was then focussed by a lens (L) onto the sample that was placed on an automatic translation stage (TS). The transmitted beam then passed through another neutral density filter (NDF), again to avoid saturation of the detector, before going to the probe detector, another large area photodiode (LAPD2). An aperture (A3) was placed in front of the probe detector for the nonlinear index of refraction measurements (closed aperture Z-scans).

As was mentioned in Section 4.1, the signals from the large area photodiodes were extremely short (~ 40 ns) and it was thus impossible to capture these signals with normal analog to digital (A2D) data acquisition cards. This necessitated the conversion of these short signals to signals that the A2D card could measure. This conversion was done by first feeding these quick signals into boxcar integrators (BC1 and BC2). The boxcar integrators operated on the principle that they select a part of an electrical pulse and output the time-integrated value of that part of the pulse as a DC signal.

The part of the pulse that is integrated can be chosen as well as the integration duration. This allows one to capture the peak values of the fast pulses from the large area photodiodes and to feed the generated DC signals to a normal A2D data acquisition card that is housed in the personal computer (PC). A further advantage of using the boxcar integrators is that, because the part of the pulse that is integrated is chosen, electromagnetic noise that is on top of the signal can be eliminated. By merely selecting a part of the pulse that clearly contains hardly any noise, a much more stable signal is achieved, with an improved signal-to-noise ratio.

The two boxcar integrators are triggered by a pulse from a fast photodiode (FPD) and the data acquisition card is triggered directly from the Excimer laser. The computer also controls the automatic translation stage.

4.3 Characterization of the experimental setup

The functioning of the components of the setup was evaluated in order to determine the influence of each component on the quality of the measurements. This was done in order to minimize or eliminate their contributions to errors. In this fashion the factors that could be included in the analysis of the data could be determined.

4.3.1 Beam quality

The theory of the Z-scan analysis was based on the assumption that the incident probe beam had a Gaussian (TEM_{00}) beam profile. This assumed the spatial profile of the energy (and thus the intensity distribution) to be Gaussian, which made the analysis possible. The Dye laser pulses used in the experiment were generally non-Gaussian, as can be seen in Figure 4-2. This illustrated the need for some technique by which to improve the beam shape, to ideally create a Gaussian beam profile.

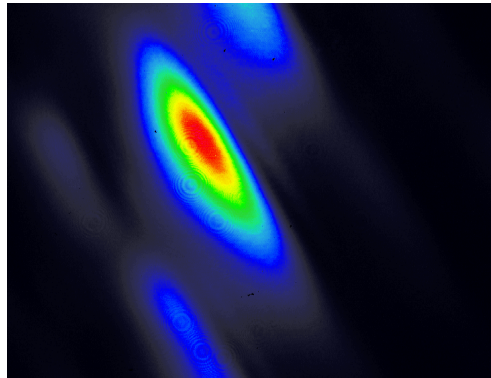


Figure 4-2: An intensity profile of the Dye laser pulse, which is clearly non-Gaussian.

Various techniques for improving the beam quality were investigated. Initially a spatial filter was inserted in the laser beam. A spatial filter works on the principle of discriminating between the different spatial modes that coexist inside a laser pulse, based on the fact that they all have different spot sizes at the focus. The spatial filter ideally only allows the TEM_{00} mode to pass through because this mode has the smallest spot size at the focus. The spatial filter focuses the beam through a very small aperture ($5 \mu\text{m}$ diameter) with the aim of letting the TEM_{00} mode pass through the aperture while blocking all the other modes.

An open aperture Z-scan was performed using this beam and the result that was obtained clearly showed two foci (two minima in a transmittance versus position graph can be seen in Figure 4-3).

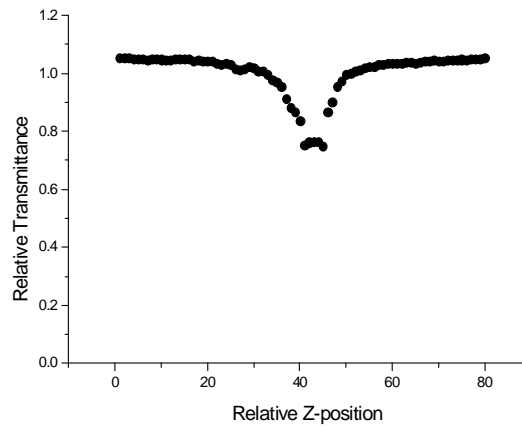


Figure 4-3: An open aperture Z-scan of C_{60} using the spatially filtered Dye laser beam showing two clear minima.

The position of the aperture with respect to the lens that focussed the beam through the aperture inside the spatial filter could be set. By changing the distance between the aperture and this lens, the relative intensities of these two foci with respect to each other changed. This indicated that the two foci were indeed created as a result of the spatial filtering. Not only did the beam show multiple foci, it was visually clear that the beam profile did not have a Gaussian intensity distribution. This can be seen in the two-dimensional image of the filtered beam, shown in Figure 4-4.



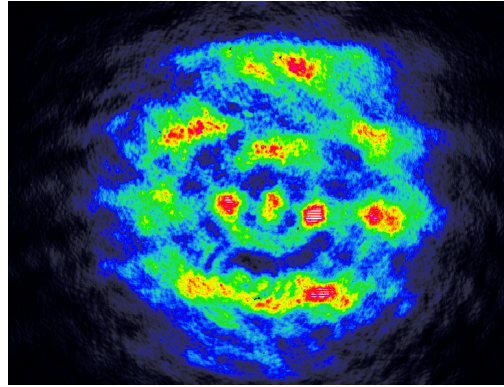


Figure 4-4: The intensity distribution of the Dye laser beam after passing through the spatial filter.

The disappointing result obtained using the spatial filter necessitated the use of another technique. Instead of trying to create a Gaussian (TEM_{00}) beam, it was decided to rather opt for a closely related beam shape, namely a clipped Airy pattern. This was the approach followed by Bum Ku Rhee *et al* [8].

A clipped Airy pattern is created by first inserting an aperture into the laser beam, thus creating a normal Airy pattern. The beam is then allowed to propagate a distance in free space. A second aperture is now inserted into the beam (see Figure 4-5). Ideally, the diameter of this second aperture must correspond to the first minimum of the Airy pattern. In this fashion only the centre maximum is allowed to propagate. This centre maximum is symmetric and has an intensity distribution close to that of a Gaussian beam.

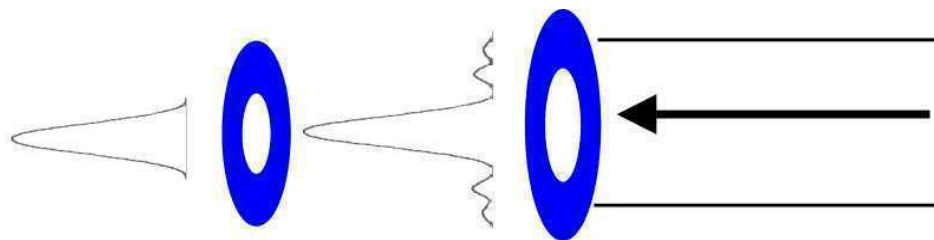


Figure 4-5: An illustration of how a clipped Airy pattern is created.

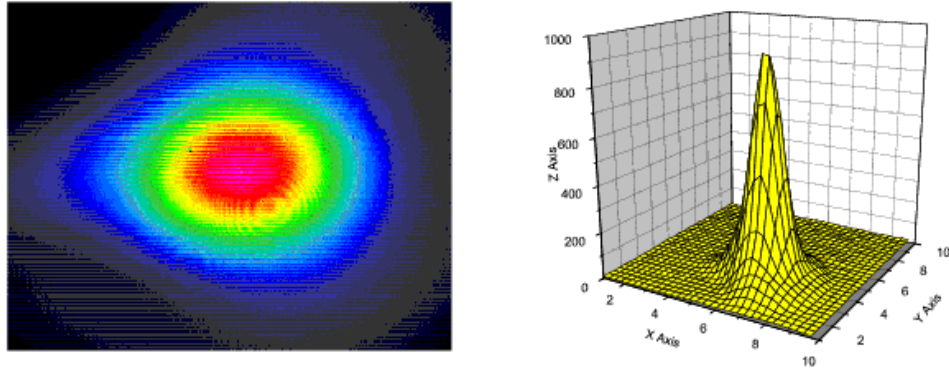


Figure 4-6: Two- and three-dimensional intensity profiles of the clipped Airy pattern used in the experiment.

This approach was followed and proved to be a very useful technique. The beam profile obtained in this manner was nearly perfectly symmetrical. It only deviated from symmetry in the extreme flanks, as can be seen in Figure 4-6.

4.3.2 Data capturing, processing and averaging

It is important to distinguish between nonlinear and linear processes when considering data processing and averaging. Nonlinear processes introduce different considerations that need to be taken into account. This will be expanded on later in this section.

A Z-scan was used to measure the nonlinear absorption or the nonlinear refraction of a sample. These are classic examples of nonlinear interactions. It was thus necessary, when dealing with the data from a Z-scan, to take these considerations into account. The data obtained from a Z-scan was a transmittance versus z -position graph. The transmittance was defined as the ratio obtained by dividing the energy measured by the probe detector by the energy measured by the reference detector. The reference detector was used to compensate for fluctuations that occurred in the laser energy on a pulse to pulse basis.

To improve the final measurement, numerous measurements were taken at each z -position, as would have been the case had this been a linear process. The number of measurements at each position determine the accuracy of the final measurement, but increase the time required to perform the experiment. If this was a normal linear process that was being investigated,

then the average of all these measurements would simply have been taken. This would have significantly improved the measurements.

This can, however, not be done in the case of a Z-scan since it is a nonlinear process that is being investigated. This implies that the average of all these measurements should not simply be taken. The measurement taken by the probe detector is the result of a nonlinear process whereas the measurement taken by the reference detector is merely the linear fluctuations in laser energy.

Nonlinear processes are intensity dependent and thus only measurements taken with exactly the same intensity at the waist should be considered together. Intensity is dependent on the spatial and temporal profiles of the laser pulse as well as the laser energy. Since only the laser energy is measured on a pulse to pulse basis (reference detector measurements) it has to be assumed that the spatial and temporal profiles of the laser pulse remain constant. This implies that measurements that originate from the same laser energy can be considered together.

Only the energy was measured, because the photodiodes that were used could not resolve the temporal profiles of the laser pulse. The photodiodes produced ~ 40 ns electrical pulses in response to ~ 10 ns laser pulses. These 40 ns electrical pulses were still too fast for the data acquisition card and thus a boxcar integrator needed to be used as well. The boxcar integrator selected a part of the electrical pulse and time integrated that part. The integrated value was sent to the data acquisition card as a DC signal. It was these values that were taken as the energy measurements.

It was of course impractical to consider measurements that were taken at exactly the same energy. As compensation, a small energy interval in the data taken by the reference detector was considered. All of these measurements taken by the reference detector inside the energy interval, had a corresponding measurement taken by the probe detector. This meant that for each small energy interval taken in the data of the reference detector, the corresponding measurements taken by the probe detector were all conducted at nearly the same energy. For each of these energy intervals in the data of the reference detector, there existed a corresponding subset of measurements in the data from the probe detector.

Each of these subsets should represent an independent Z-scan, each conducted at a slightly different energy. This is illustrated in Figures 4-7 and 4-8. Figure 4-7 shows the reference

energy distribution for a Z-scan and two energy intervals. Figure 4-8 shows the probe energy distribution and the two Z-scans that should originate when taking the corresponding measurements to those inside the energy intervals in Figure 4-7. The measurements inside each of these subsets should still contain some fluctuations, but because these measurements originated at nearly the same intensity, they could now be averaged, as long as it was done only within a subset.

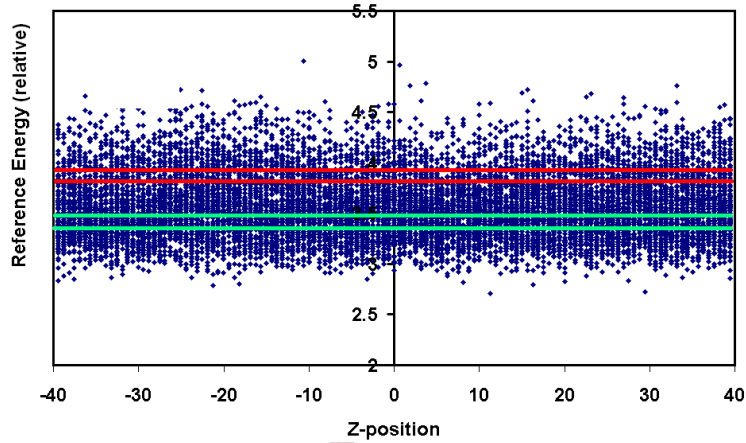


Figure 4-7: The energy distribution as measured by the reference detector. A hundred samples per z-position were taken. Energy intervals are also indicated.

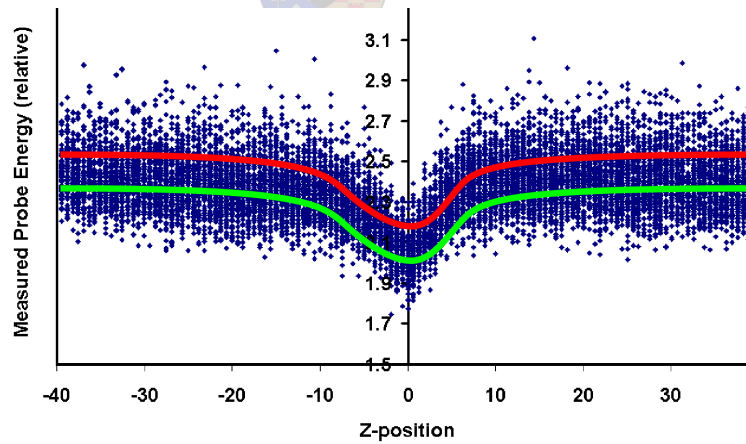


Figure 4-8: The measurements taken by the probe detector. The coloured lines correspond to the the energy slices shown in Figure 4-7.

This treatment is only correct if the fluctuations that occurred in the measurements were only the result of the pulse to pulse fluctuations in energy. For the measurements that were taken using the Dye-laser, the fluctuations also originated as a result of changes in the temporal and spatial profiles of the laser pulse. These pulse to pulse variations in spatial and temporal profiles of the laser pulses resulted in changes in peak intensity and thus influenced the nonlinear absorption that occurred. Since the detectors used in the Z-scan merely measured the energy and not the peak intensity, these fluctuations could not be accounted for by this method of taking small energy intervals. The fluctuations that still existed can be seen in Figure 4-9.

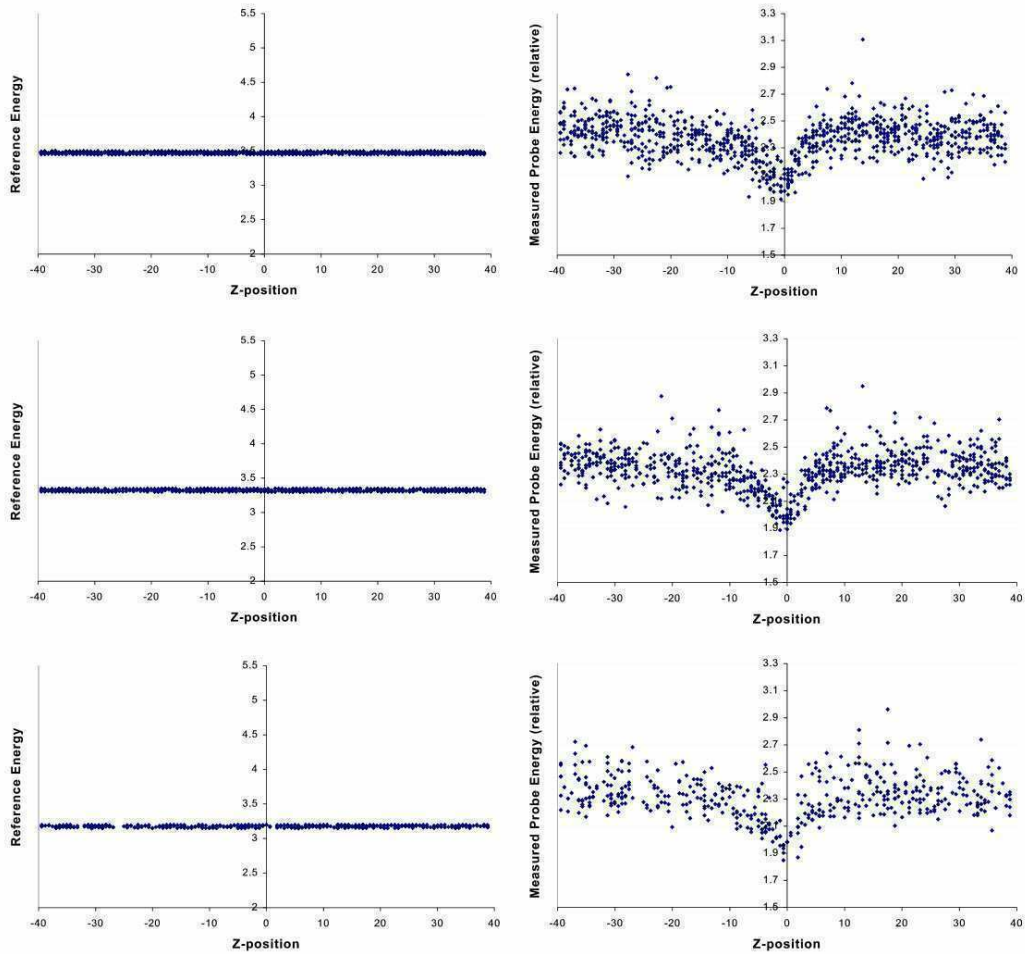


Figure 4-9: Three energy intervals in the reference detector's data (left) and the corresponding data of the probe detector (right).

In order to obtain more accurate measurements, improvements in laser stability are required. This includes both spatial and temporal stability. The results could clearly not be improved by improving the data acquisition.

Because the measurements taken by the probe detector in each of the subsets were taken at nearly the same energy, and because the other fluctuations could not be eliminated in these subsets of measurements, nothing else could be done other than to average these measurements inside these subsets. The nonlinear absorption coefficient or the nonlinear index of refraction could now be extracted from each of these averaged subsets of data. The fact that each actual Z-scan produced a number of effective Z-scans allowed for normal statistical processes for error determination that would normally require multiple scans. This was the approach followed in determining the error bars on the measurements that were conducted.

This approach is the correct way to process data when dealing with measurements of nonlinear effects. The reality is that the advantage of this approach over normal averaging is not always apparent because the fluctuations that occur in the measurements can have different origins, as was the case in these Z-scans.

4.3.3 Sample thickness

As was mentioned in Section 3.2.1, one of the experimental considerations was the sample thickness. This thickness must be less than the Rayleigh length of the focussed laser beam. This is necessary for the sample to be considered thin and for the nonlinear processes to be considered to occur at a single position and not to be spread across the length of the sample. An added advantage is that not a large amount of sample material is necessary for a Z-scan. In the experiments conducted with samples in solution, the sample length was 2 mm while the Rayleigh length was 3.4 mm. For the experiments conducted with ZnO, the sample length was 0.5 mm, with the same Rayleigh length used.

4.3.4 Background

It is possible that poor sample quality, in the case of solid samples like crystals, or poor cuvette quality, in the case of liquid samples, can mask the nonlinear effects that occur in a sample. It is possible to eliminate these masking effects by performing two Z-scans, one at the desired

energy for the experiment and one at a very low energy. The data obtained from this second "background" scan [5] must then be subtracted from the data obtained from the high energy scan. In this fashion the effects attributed to the sample quality are eliminated. This can even be done for large surface disturbances ($\Delta\phi_{\text{surface}}$ of up to π), as long as the surface disturbances do not change the circular symmetry of the beam or cause beam steering.

4.3.5 Solvent effect

When performing a Z-scan on samples that are in solution, it is important to consider the effect of the solvent. This will of course depend on the solvent used. The effect of the solvent cannot be eliminated by performing a low intensity background Z-scan. In order to determine the effect of the solvent it is necessary to perform both open and closed aperture Z-scans of the pure solvent at the same energy at which the experiment is to take place. Toluene was used as solvent for C_{60} . It is known that it displays nonlinear refraction [9]. The results obtained for both nonlinear absorption and refraction of toluene will be presented in the experimental results of C_{60} (Section 5.1.2).

4.3.6 Nonlinear refraction in cuvette material (quartz)

Another factor that may influence the measurements is the quartz cuvette in which the sample is placed. Depending on the sample being investigated, the quartz cuvette may have a similar influence to that of the solvent, either masking or accentuating the nonlinear refractive index measurement being conducted. In the case of these measurements it was, however, not necessary to consider the effect of the nonlinear refraction in the quartz since its nonlinear index of refraction is roughly four orders of magnitude smaller than that of C_{60} [10].

4.3.7 Stray reflections

The use of photodiodes as detectors introduce experimental considerations because of the mere nature of photodiodes. These detectors are easily saturated and therefore care must be taken to ensure that this does not happen. Furthermore, stray reflections can be a problem. As the sample is moved, the reflections from the sample change in direction and position. The result of this is that the light that reaches the detector can change as a function of the position of

the sample because of stray reflections. This introduces false trends in the data obtained from a Z-scan. These trends can be corrected for by performing a background scan, but a better solution is to screen the detectors from all stray reflections and ensure that only transmitted light through the sample reaches the detector. In the experimental setup used the detectors were screened by placing shielding material around the beam path leading to the detectors.

4.3.8 Optical damage in cuvette

Quartz has a relatively low damage threshold. This puts a limitation on the intensity range over which the investigation of a sample can be done when the sample is a liquid. More specifically, it means that energies below $50\mu\text{J}$ [11] must be used, which translates into intensities below 220 MW/cm^2 . This low damage threshold limits the sensitivity of the experiment as the nonlinear properties of trace concentrations of a sample under investigation cannot be measured. Practical optical limiters need to be effective already at relatively low intensities, which implies that for the investigation of optical limiters, this upper energy boundary is not limiting.

4.3.9 Nonlinear scattering

A secondary effect that enhances the apparent nonlinear absorption is that of nonlinear scattering, which occurs when the intensity inside the sample under investigation is high enough to create a localized plasma. This plasma then acts as a source for scattering centres. The scattering reduces the transmission through the sample and thus increases the apparent absorption. Although nonlinear scattering is a useful process when considering a material for optical limiting applications, it makes it impossible to extract the nonlinear properties of material from a Z-scan, as it is not possible to separate the effects in the data. An example of a Z-scan that contains nonlinear scattering can be seen in Figure 4-10.

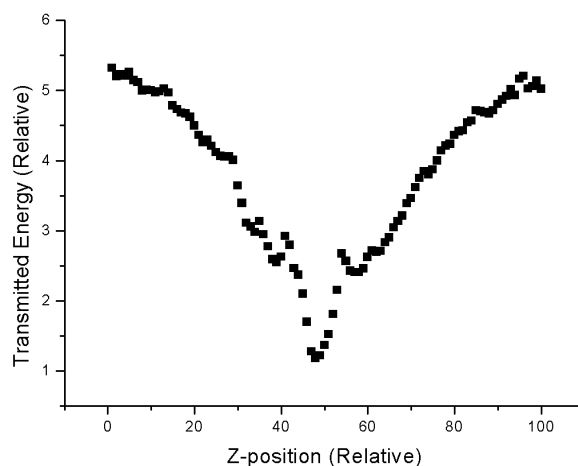


Figure 4-10: A Z-scan showing the influence of nonlinear scattering.

The strong nonlinear absorption is visible in Figure 4-10 is because of the high energy used in the Z-scan. The sudden decrease in transmittance close to the focus is indicative of plasma formation. This was also visually confirmed by bubbles forming in the sample.

4.3.10 Cuvette type

The choice of cuvette can influence the measurements. In general, the solvents used to prepare the samples are volatile. It is thus necessary to have a cuvette which can seal tightly to ensure that the concentration of the sample remains constant and known during a measurement. A further problem that a sealed cuvette helps to eliminate is that of oxidation (see Section 5.3.1 for an example of such a sample). This is a problem that occurs with some samples, especially when the sample is in an excited state, as is the case during a Z-scan.

The type of material used for the cuvette is also important. Good quality quartz with a high transmission and large spectral range is essential. The quartz must have negligible influence on the transmitted light. Preferably no fluorescence must occur in the quartz. This ensures that the attenuation that occurs is a result of the sample and not the cuvette. This also enables the expansion of the setup to look at the fluorescence spectrum of a sample while performing the Z-scan (see the section on future work, Chapter 6).

4.3.11 Iris for closed aperture Z-scans

In this investigation the focus was on determining the nonlinear absorption coefficients of various materials. In order to show the versatility of the setup it was shown that the setup could be used to determine the nonlinear index of refraction of a sample through performing a closed aperture Z-scan. Performing a closed aperture Z-scan entails placing an aperture in front of the probe detector. The placement of this aperture is extremely critical. Any deviation from perfect alignment introduces asymmetry in the data which masks the nonlinear refraction. By placing the iris in front of the detector, a small part of the transmitted laser pulse is sampled. Ideally the exact same part of the beam must be sampled each shot, but because of deviations in spatial distribution of the laser beam on a shot to shot basis, this is not possible. This results in fluctuations in the measured data that contribute to the error in the signal.



Chapter 5

Material descriptions and experimental results

Two materials were investigated extensively with the Z-scan setup, C_{60} and ZnO. Since C_{60} is known to have strong nonlinear properties most of the emphasis was placed on this material. The properties of C_{60} have been well analyzed and documented in the literature [9][11][15][16][17], making it an ideal candidate for testing and evaluating the experimental setup.

The ZnO sample is a crystal while the C_{60} is analyzed in a solution. This makes ZnO useful to illustrate the versatility of the setup for measuring the nonlinear properties of different types of samples. ZnO is also an interesting sample because it has some unusual characteristics; it is a transparent semi-conductor which is sufficiently conducting to be used as electrodes. This makes it a very useful material in solar cell construction, where it is used for the contacts on the cell. Furthermore, ZnO shows high chemical stability and has a high melting point (~ 2300 K) [12]. This makes it an ideal material for use as an optical limiter. It is however still difficult to produce large, single crystals, but this is a technological problem.

Lastly, two novel materials, poly(dioctyl-fluorene) and CdS quantum dots, were investigated. Both these samples proved difficult to analyze, for various reasons (which will be expanded on later), and thus only preliminary investigations were conducted.

5.1 C₆₀, the Buckminsterfullerene

5.1.1 Nonlinear absorption in C₆₀

Since their discovery in 1985 [13], fullerenes (of which C₆₀ is the most common) have been heavily investigated due to their unique three-dimensional, conjugated (double-bond containing) π -electron system. It is known that delocalized π -electrons provide exceptionally large nonlinear optical responses, and this makes fullerenes like C₆₀ good candidates when looking for a material to be used as an optical limiter or a material with an intensity-dependent refractive index. This made it an ideal candidate for testing and evaluating the effectiveness of the experimental setup. A slice through the electron shell of the C₆₀ molecule can be seen in Figure 5-1, which shows the spherical symmetry of the molecule [14].

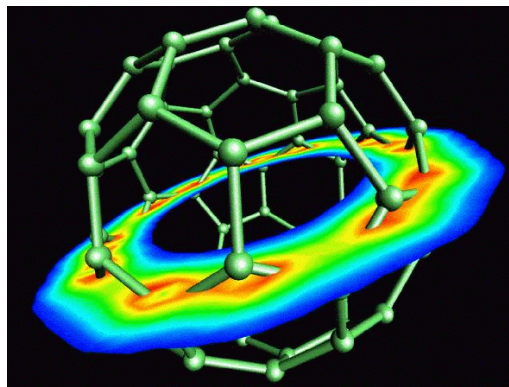


Figure 5-1: A figure showing the structure of a C₆₀ molecule with a single plane of the delocalised π -electrons visible, taken from [14].

The induced absorption of the C₆₀ molecule can best be described by a five-level model [16][15]. The simplified energy level diagram can be seen in Figure 5-2. Each electronic state of the molecule gives rise to a manifold of associated vibrational states, indicated by the thin lines above each of the thicker ones in Figure 5-2. The thick lines represent the zero-vibrational electronic states.

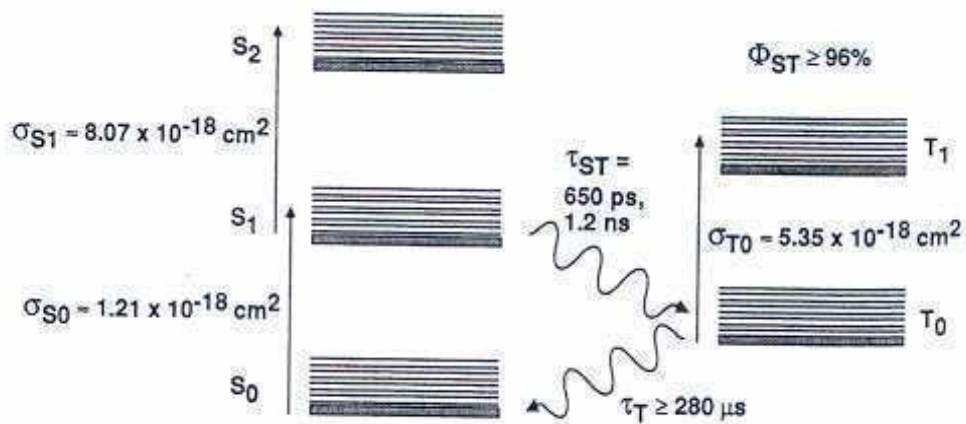


Figure 5-2: A simplified 5-level energy diagram of the C_{60} molecule, taken from [15].

C_{60} has singlet and triplet excited electronic states, the first triplet state lying energetically below the first excited singlet state. Absorption of photons by the molecule excites electrons in the ground state, S_0 , to one of the molecular vibrational levels of the first excited singlet state, S_1 . These states relax very quickly (~ 1 ps) [16] to the lowest vibrational level of the first excited state. Subsequent absorption of another photon by the molecule can further excite one of the electrons that is in the excited state S_1 to an even higher singlet state, S_2 . The excited state S_1 can also return to the ground state through internal conversion, or can undergo an intersystem crossing to the first triplet state, T_0 . Absorption of another photon by the molecule can excite an electron in state T_0 to the first excited triplet state, T_1 .

The intersystem crossing rate is very fast (650 ps - 1.2 ns), with quantum efficiency close to unity [17], indicating that nearly each radiatively produced exciton in the S_1 state follows the channel via the T_0 state and does not relax directly back to the S_0 state. The radiative decay of an exciton from the triplet state T_0 to the singlet ground S_0 state is spin-forbidden, which results in an extremely long lifetime, in the order of 280 μ s. Furthermore, the decay from the higher states (S_2 and T_1) is very rapid [16], which has the result that the states S_1 and T_0 are effectively not depopulated by the laser pulse. This implies that there will be a high population in S_1 and T_0 for the duration of the laser pulse. Because these two states have significantly

higher absorption cross-sections than the ground state [16] (for wavelengths around 532 nm), an increase in absorption is achieved. This accounts for the intensity dependent (nonlinear) absorption and thus the optical limiting behaviour of C_{60} .

5.1.2 Experimental results for C_{60}

C_{60} was investigated using the Z-scan setup described in Section 4.2. Figure 5-4 (shown on Page 55) shows a typical Z-scan performed on a C_{60} solution. This specific result was obtained using a 0.4 mM solution of C_{60} in toluene as sample. This concentration was chosen because it resulted in nonlinear absorption of 17% (absorption had to be kept below 23%, see Section 3.2.2) at energies that allowed for sensitive measurements with the detectors and neutral density filters chosen and without any other nonlinear effects like nonlinear scattering.

The data were obtained by measuring the transmitted and reference energy at each z-position over 100 laser pulses. The sample was moved 130 steps of 0.63 mm each. This amounted to a distance which ensured that the linear and nonlinear regions were sufficiently covered. The step size chosen equated to a quarter revolution of the stepper motor used to drive the translation stage.

The laser used was the XeCl Excimer laser pumped Dye laser (Coumarin 540 used as dye), tuned to 540 nm. The pulse length (full width at half maximum) of the Dye laser was measured using a fast photodiode and was found to be 10 ns. The energy used in the measurement was 3 μ J.

Experimentally, it was quite difficult to measure the Rayleigh length of a tightly focused pulsed laser beam accurately. The Rayleigh length was therefore extracted from the fit on the data from the Z-scan rather than measuring it with a knife edge or a slit. This seemed to be standard practice according to the literature [11]. The Rayleigh length of the focused beam (a 100 mm lens was used to focus the beam) was determined as 3.4 mm, which related to a beam waist at the focus of $\omega_0 = 24 \mu\text{m}$.

The intensity was calculated by dividing the pulse energy (3 μ J) by the product of the pulse length (10 ns) and the cross-sectional area of the pulse at the focus ($\pi\omega_0^2$). This yielded an intensity at the focus of 16 MW / cm².

Equation 3.39, shown here again as Equation 5.1, was fitted to the data, replacing the

infinite sum with a sum over the first 60 terms.

$$T(z) = \sum_{m=0}^{60} \frac{[-q_0(z)]^m}{(m+1)^{\frac{3}{2}}} \quad (5.1)$$

$$q_0 = \frac{\beta I_0 L_{\text{eff}}}{1 + \frac{z^2}{z_0^2}} \quad (5.2)$$

$$L_{\text{eff}} = \frac{1 - e^{-\alpha L}}{\alpha} \quad (5.3)$$

The rationale for this was discussed at the end of Section 3.2.2 and shown in Figure 3-8. The fitting parameters were the nonlinear absorption coefficient and the Rayleigh length. The fit was done using the Levenberg-Marquadt method, which is a standard way of minimizing nonlinearities. The method consists of taking an estimation for the values of parameters that need to be fitted. The deviation from the data is then expressed as a function of the fit parameters and this function is then minimized through an iterative process.

The reason for taking 100 measurements per position was to improve the signal-to-noise ratio and to decrease the error of measurement. It is important to note that the experiment deals with a nonlinear process, which makes it impossible to merely take the average of the ratios of the measurement of the probe detector and the reference detector, as was mentioned in Section 4.3.2. In fact, it necessitates the categorizing of the data according to very narrow energy regimes to ensure sensible data analysis, as was explained. The measurements taken by the reference detector were divided into narrow energy sections and the corresponding measurements on the probe detector were then grouped together. This effectively yielded multiple scans from a single Z-scan, each at a slightly different energy. When all these "scans" were normalised, the error on each measurement of each of the "scans" could be determined. By combining these "scans" an error bar for the measurement could be determined and this was done in the standard way of considering the mean deviation.

As was discussed in Sections 4.3.4 and 4.3.5, it was necessary to perform a background scan, using only the solvent, in order to eliminate any false signals. Figure 5-3 shows such an open aperture Z-scan conducted with toluene as sample. It can be clearly seen that toluene displays no nonlinear absorption and that any background effect is minimal. This result implies that future open aperture Z-scans can be conducted with confidence and without background scans,

as the background effects are negligible and need not be taken into account.

The resultant Z-scan obtained from the conditions described above is depicted in Figure 5-4. This enabled the extraction of the nonlinear absorption coefficient from the data, which was found to be, $\beta = 0.3 \text{ cm} / \text{MW}$.

The same process was followed for different concentrations of C_{60} in toluene solutions, at the slightly lower energy of $2.5 \mu\text{J}$. For each of these samples the nonlinear absorption coefficient was extracted and plotted against the concentration of the sample. The result can be seen in Figure 5-5. As expected, according to the literature [11], the graph shows a clear linear trend.

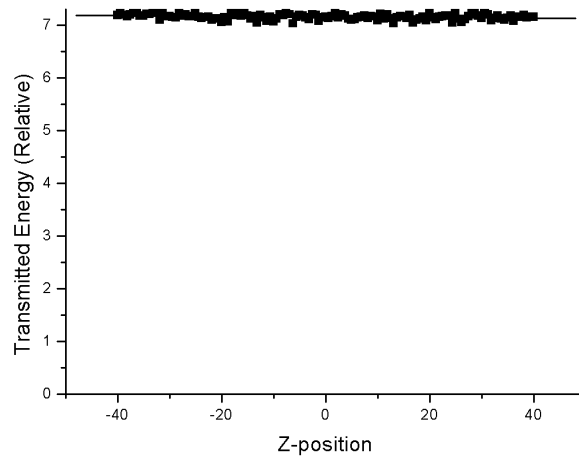


Figure 5-3: An open aperture Z-scan conducted with pure toluene as sample to illustrate the low background signal.

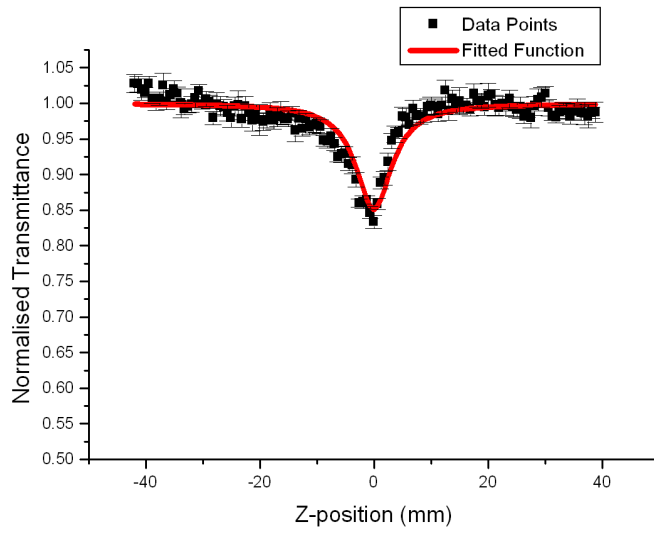


Figure 5-4: A Z-scan of C_{60} along with the fitted function on the data. Error bars are also shown.

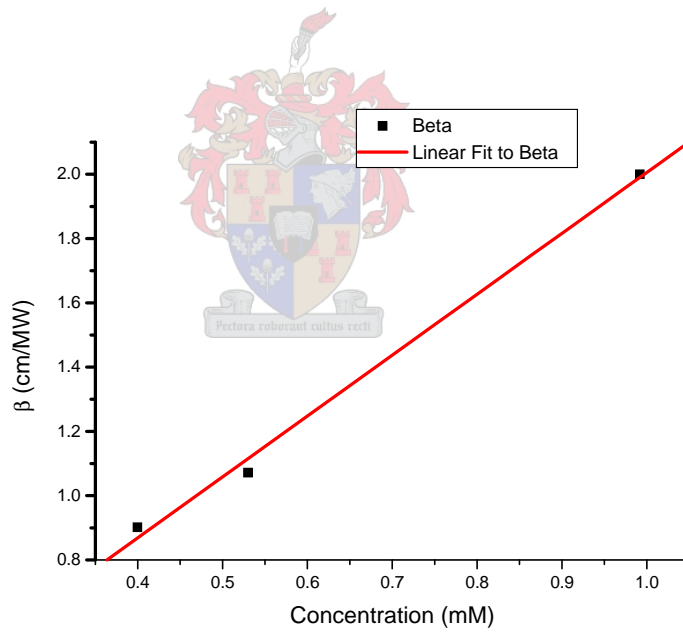
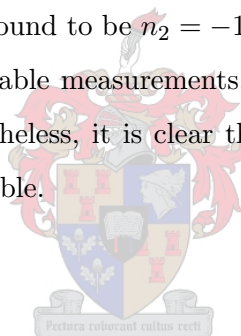


Figure 5-5: A graph depicting the linear dependence of the nonlinear absorption coefficient, β , on the C_{60} concentration.

As an example of the versatility of the setup the nonlinear index of refraction of C_{60} was investigated. Because of the difficulty involved with the alignment of the iris, it was difficult to produce repeatable and thus quantitative results. It could, however, be clearly seen that the sample displayed nonlinear refraction. Figure 5-6 shows the data from an open aperture Z-scan of a 2 mM solution of C_{60} in toluene. The measurements were conducted with a Dye laser energy of $18 \mu\text{J}$, since the nonlinear index of refraction measurements did not require the nonlinear absorption to be kept below 23%. Figure 5-7 shows the accompanying closed aperture Z-scan. This was performed on the same sample with the same energy. An iris was inserted in front of the probe detector, reducing the transmitted energy to 10% of the original value in the linear regime ($S = 0.1$). Although it is difficult to see, a slight shift in symmetry is visible as a result of the nonlinear refraction. Dividing the data from the closed aperture Z-scan by the data from the open aperture Z-scan (Figure 5-7 divided by Figure 5-6) yields Figure 5-8, in which the nonlinear refraction is clearly visible. By taking the difference between the peak and valley transmittance, and using Equation 3.20 the nonlinear index of refraction could be determined. This was found to be $n_2 = -1.2 \times 10^{-6} \text{ cm}^2 / \text{W}$. As mentioned earlier, it was difficult to perform repeatable measurements, and thus not too much emphasis should be placed on this value. Nevertheless, it is clear that by using this experimental setup, the nonlinear refraction is clearly visible.



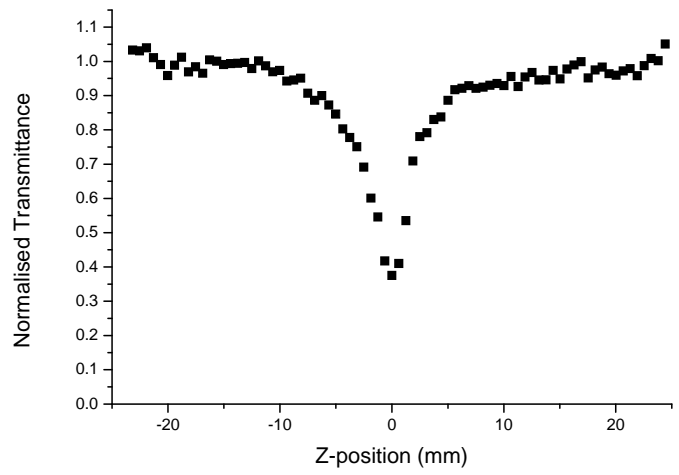


Figure 5-6: The open aperture Z-scan performed on C_{60} used for the nonlinear index of refraction measurement.

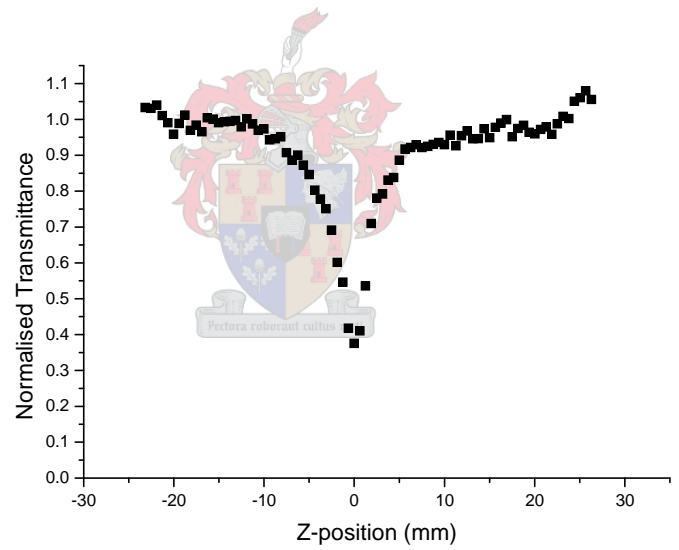


Figure 5-7: The closed aperture Z-scan performed on C_{60} used for the nonlinear index of refraction measurement.

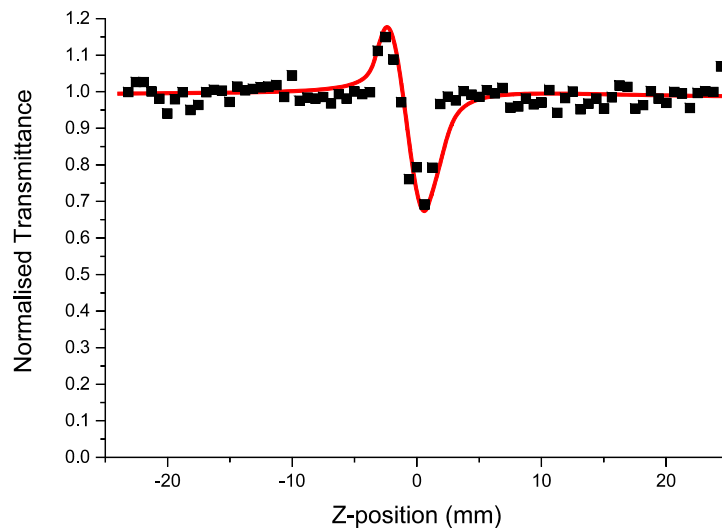


Figure 5-8: Data obtained from a combination of a closed and open aperture Z-scan (Figures 5-6 and 5-7) for determination of the nonlinear index of refraction of C_{60} .

As was stated in Section 4.3.5, toluene displays nonlinear refraction. This necessitates that the nonlinear index of refraction of toluene first be measured and included in the analysis when measuring the nonlinear index of refraction of C_{60} . One expects the contribution from toluene to be very small as its nonlinear index of refraction is about three orders of magnitude smaller than that of C_{60} [18]. A closed aperture Z-scan of toluene was performed with a slightly higher energy ($23 \mu\text{J}$ compared to $18 \mu\text{J}$). The result can be seen in Figure 5-9. It is clear that no significant nonlinear refraction occurred under these experimental conditions. This again had the fortunate implication that it was not necessary to incorporate the nonlinear refraction of toluene into the analysis of C_{60} , similar to the background scan for the open aperture Z-scan.

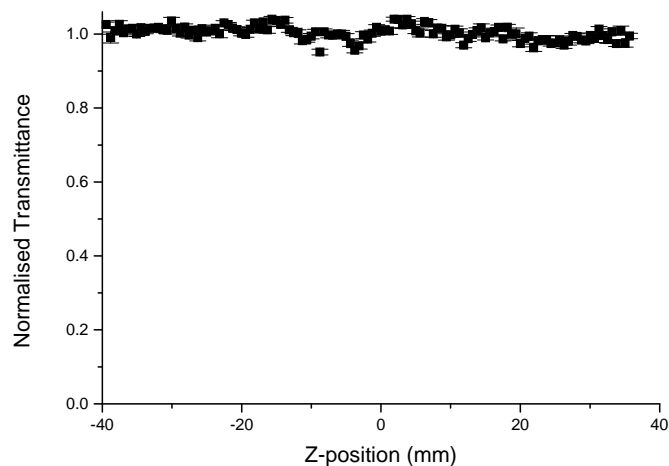


Figure 5-9: A closed aperture Z-scan of pure toluene showing how little the nonlinear index of refraction of toluene influences the measurement of that of C_{60} 's nonlinear index of refraction.

5.2 Experimental results for single crystalline ZnO

To investigate the versatility of the setup it was decided to measure the nonlinear properties of single crystalline ZnO. The same setup was used as for the measurements done with C_{60} as sample. The only difference was that a new sample holder had to be constructed to hold the crystal in place. This implied that all the experimental considerations that were applicable to the C_{60} measurements still held, barring those pertaining to possible problems with the cuvette.

With the crystal, one also had to be careful about inducing optical damage, although this was unlikely since ZnO has a high damage threshold; it experiences no damage at intensities of up to $70 \text{ GW} / \text{cm}^2$ [19]. With this in mind, the nonlinear absorption coefficient and nonlinear index of refraction of single crystalline ZnO was measured.

Nonlinear absorption

For the experiment, a 1 cm^2 crystal of 0.5 mm thickness was used. Because the sample was so thin it was necessary to use high laser energy ($110 \mu\text{J}$) to obtain significant nonlinear absorption.

The Dye laser wavelength was still 540 nm. With these parameters an intensity of $0.5 \text{ GW} / \text{cm}^2$ was obtained. The resultant open aperture Z-scan is shown in Figure 5-10. It was possible to extract the nonlinear absorption coefficient, which was found to be $\beta = 49 \text{ cm} / \text{GW}$.

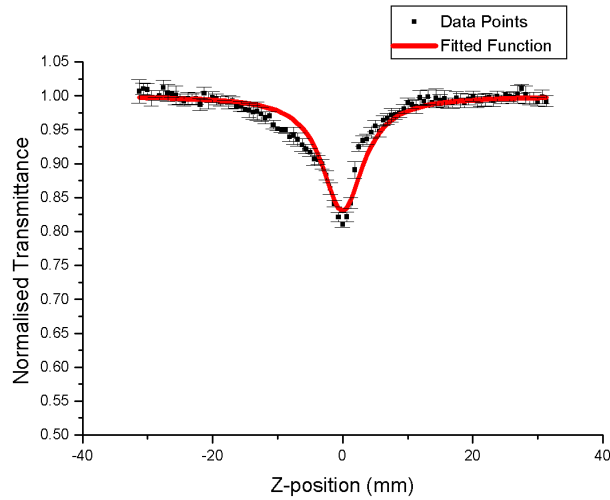


Figure 5-10: A closed aperture Z-scan of ZnO. The fitted function and error bars are also shown.

Nonlinear refraction

For the measurement of the nonlinear index of refraction of ZnO, the same problem of sensitivity was encountered as was the case with C_{60} . Figure 5-11 shows the Z-scan with an open aperture and Figure 5-12 the corresponding Z-scan with an aperture in place in front of the probe detector. The energy used in the two Z-scans was $55 \mu\text{J}$. A slight change in the diameters of the apertures shaping the beam allowed for a tighter focus and thus an increase in the intensity at the focus. This is why the energy used in these Z-scans was less than what was used to determine the nonlinear absorption coefficient, although nearly the same nonlinear absorption was achieved. The aperture that was placed in front of the detector allowed about 10% of the energy to be transmitted in the linear regime ($S = 0.1$). Figure 5-13 shows the result after dividing the data obtained from the closed aperture Z-scan by the data from the open aperture Z-scan (Figure 5-12 divided by Figure 5-11). Again, repeatability was difficult and thus not

to much emphasis should be placed on a value for the measurement. The value was therefore not determined as it would have no real significance. The effect of nonlinear refraction on the other hand was clearly visible.

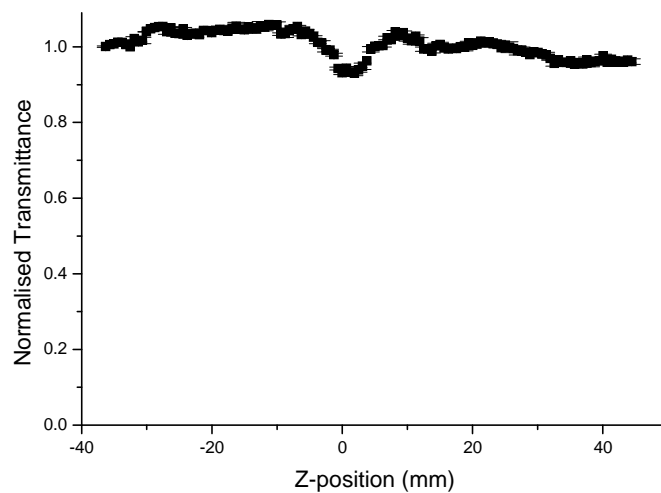


Figure 5-11: An open aperture Z-scan of ZnO.

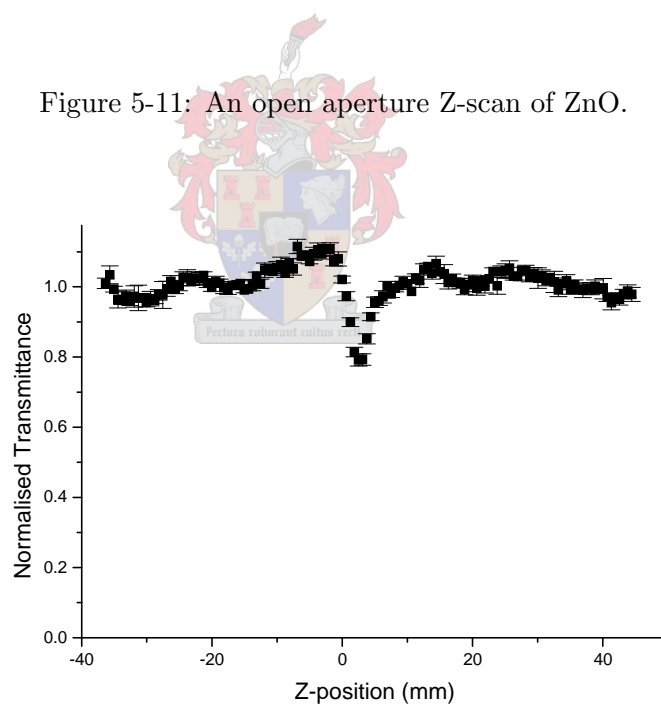


Figure 5-12: A closed aperture Z-scan of ZnO.

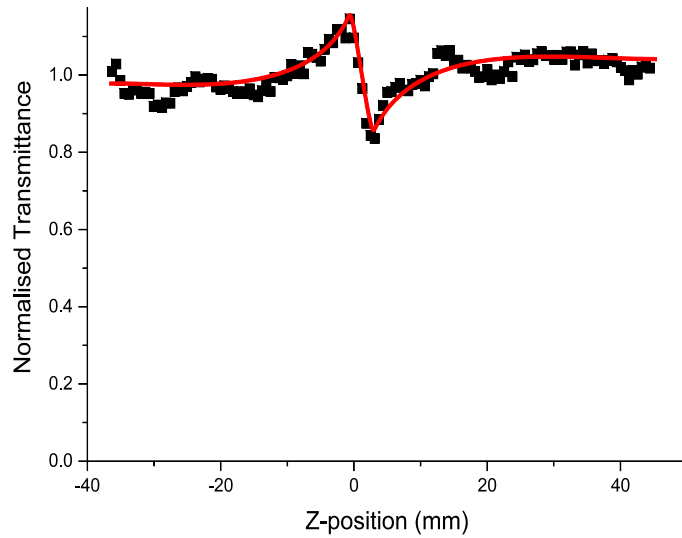


Figure 5-13: The resultant graph after dividing the closed aperture Z-scan (Figure 5-12) of ZnO by the open aperture Z-scan (Figure 5-11) of ZnO.

The fluctuations that occurred in the linear region were as a result of the fluctuations in the spatial energy distribution of the laser beam. This was explained in Section 4.3.11. This resulted in the limited accuracy of these measurements.

5.3 Experimental results of two novel materials

During the investigation of C_{60} and ZnO, other novel materials with strong nonlinear properties became available and were investigated. These included poly(dioctyl-fluorene), a large polymer, and CdS quantum dots. The CdS sample is referred to as quantum dots because of the size of the particles. They are all of the order of hundreds of nanometers in diameter. Because of various complications with these samples, which will be expanded on in the next two sections, only cursory investigations were performed on these samples. These investigations did, however, illustrate some of the difficulties that can be encountered whilst carrying out a Z-scan.

5.3.1 Poly(dioctyl-fluorene)

The photonics industry is always looking for materials with large nonlinear optical responses to be used for, amongst others, optical switches. Much interest has been placed on conjugated polymers that have extended delocalized π -electrons along their linear backbone [20]. Polyfluorenes are a class of polymers that includes prime examples of such compounds; they display very strong nonlinear absorption [20]. This was the reason for investigating one such compound, poly(dioctyl-fluorene), with the Z-scan technique. The monomer of poly(dioctyl-fluorene) can be seen in Figure 5-14.

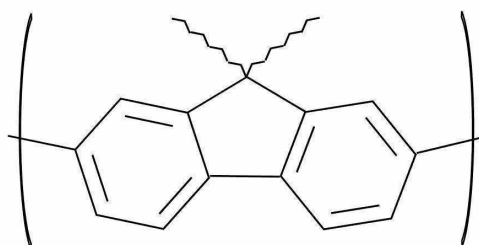


Figure 5-14: A schematic representation of the monomer of poly(dioctyl-fluorene).

A solution (3×10^{-7} M) of poly(dioctyl-fluorene) in chloroform was prepared and analyzed using the same Z-scan setup employed to analyze C_{60} and ZnO. The sample was placed in a sealed quartz cell to limit the effect of oxidation, which is a problem with poly(dioctyl-fluorene). The Dye laser energy was attenuated to $9 \mu\text{J}$ which resulted in nonlinear absorption of about 7%. The same data capturing technique as used for C_{60} and ZnO was employed here (see Section 4.3.2). The result of the Z-scan can be seen in Figure 5-15. This allowed for the nonlinear absorption coefficient to be extracted from the functional fit on the data. From the fit the value of $8 \times 10^{-2} \text{ cm / MW}$ was obtained for β .

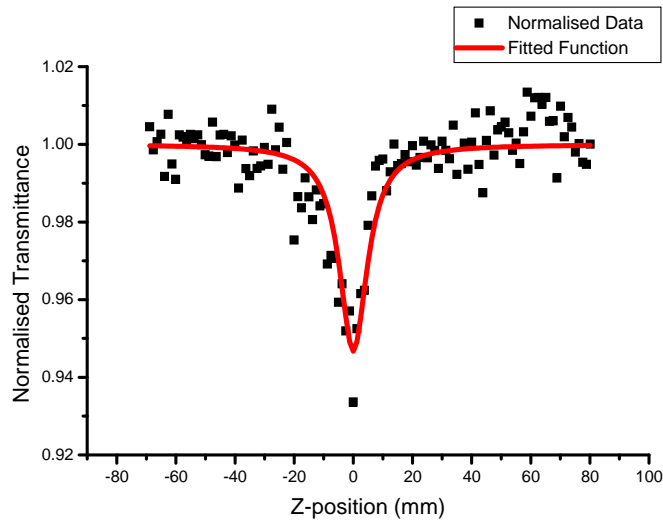


Figure 5-15: The data from a Z-scan of poly(dioctyl-fluorene) as well as the fit to the data.

One of the secondary effects that was seen during the investigation of poly(dioctyl-fluorene) was that if the sample was exposed to air and was irradiated, the transmission changed with time. This effect was attributed to oxidation of the sample and was investigated. The sample was placed in a cuvette that was open to the air. It was then placed at the focus of the setup and the transmittance as a function of time, rather than position, was measured. The sample was irradiated for approximately 75 minutes. The energy per pulse of the laser was $10 \mu\text{J}$ and the repetition rate was 10 Hz. The result of this measurement is shown in Figure 5-16. A functional fit was performed on the data to try to obtain information on the temporal dependence of the transmittance. The function fitted was chosen because of the shape of the data. No assumption was made of the different processes involved or the temporal dependence. The function that was chosen was

$$T(t) = A_0 e^{-t/A_1} + A_2 (1 - A_3) e^{-t/A_4} \quad (5.4)$$

and it fitted the data very well (Figure 5-16). The two exponential functions contained in Equation 5.4 seemed to indicate that there are two different processes involved in the photo-

oxidization of the sample. Without additional information about the chemistry involved it would be mere speculation to elaborate on these processes at this point. Values for the constants were extracted from the fit and are of academic interest should further analyses be carried out. The values were found to be: $A_0 = 0.024$, $A_1 = 317$, $A_3 = 1.01$, and $A_4 = 2484$.

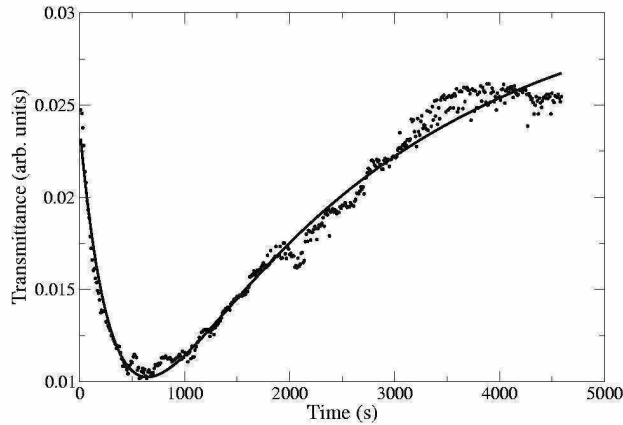


Figure 5-16: A plot of the time-dependent transmittance of poly(dioctyl-fluorene) as well as a fit to the data.

The oxidized sample was further investigated using the Z-scan setup. Two open aperture Z-scans, one at low energy ($7.5 \mu\text{J}$) and one at a relatively high energy ($19.7 \mu\text{J}$), were performed on the oxidized sample to see if it displayed any nonlinear absorption. Figure 5-17 shows clearly that the sample displayed no nonlinear absorption after it had been oxidized. If one then considers the fact that the nonlinear optical properties of poly(dioctyl-fluorene) are as a result of the delocalized π -electrons then it is a fair assumption that it is these electrons that are involved in the oxidation of the sample, as the oxidized sample displays no nonlinear optical effects.

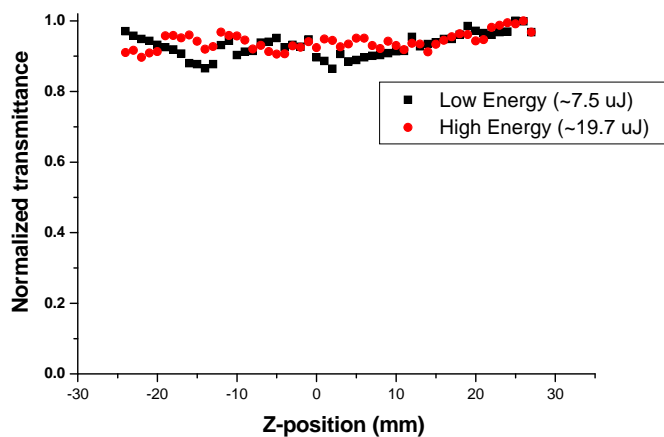


Figure 5-17: Two Z-scans of poly(dioctyl-fluorene) after oxidation.

5.3.2 CdS quantum dots

The CdS quantum dots are so called nano-particles with varying sizes, but the majority of them are smaller than a micron in diameter. Because of the structure of the particles they are highly insoluble and merely form a suspension in a non-polar solvent. This fact presents a major problem if a sample is to be investigated since a solution of the sample to be analyzed first needs to be prepared. Toluene was used as "solvent" in the investigation to form the suspension. The investigation was conducted using the same Z-scan setup as described for C₆₀, ZnO and poly(dioctyl-fluorene), the only difference being that the wavelength used was now 455 nm. The results of a Z-scan performed on a suspension of CdS quantum dots using 12 μ J of energy can be seen in Figure 5-18.

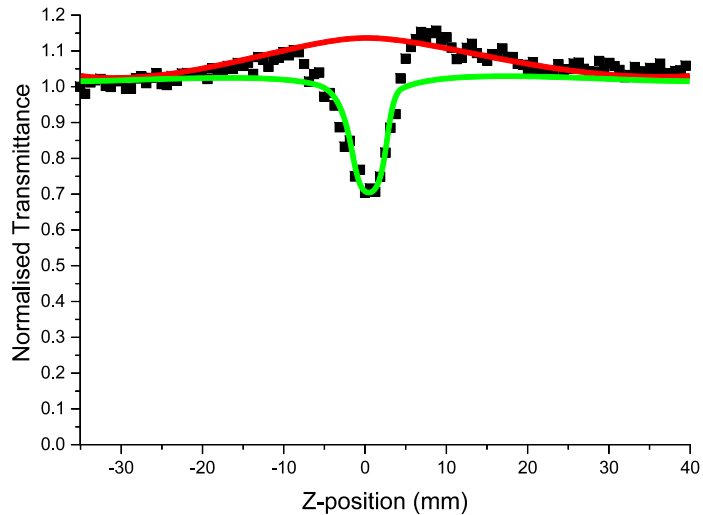


Figure 5-18: Data from a Z-scan conducted on CdS quantum dots in suspension. The two coloured lines show the two clear trends that are visible.

From the data it can be seen that the transmittance first increased as the sample approached the focus, until nonlinear absorption started to dominate. The transmittance was again higher directly after the focus than in the normal linear region. This indicated that there were clearly two different processes involved, indicated by the green and red lines in Figure 5-18. The green line indicates normal nonlinear absorption. The red line indicates a competing process. The mechanism behind this secondary process is not yet understood. One theory is that it is a decrease in scattering as a result of the decrease in beam size that accounts for the increase in transmittance. This will have to be tested by looking at the amount of scattered light from the sample as a function of position.

The fact that the sample is a suspension complicates matters. During a Z-scan the sample precipitated, effectively changing the concentration. A Z-scan was therefore not conducted on a sample with a constant concentration, making analysis of the data difficult.

Chapter 6

Conclusions

The theory underlying the nonlinear processes that occur in matter was investigated and analyzed where it applies to nonlinear refraction and nonlinear absorption. A summary of relevant theoretical considerations was presented. The Z-scan technique was chosen as the method for measuring the abovementioned nonlinear properties. To this end a theoretical analysis was performed of how the technique is utilized to measure the nonlinear index of refraction and the nonlinear absorption coefficient and was presented here. The experimental considerations and obstacles were investigated and highlighted. This allowed for the implementation of the theory into an experimental setup.

The Z-scan technique which was analyzed in detail was then implemented in a Z-scan setup with the aim of determining the nonlinear properties of selected materials. The setup was constructed, systematically improved and categorized in order to perform repeatable measurements. For the characterization a suitable sample had to be chosen and C_{60} was decided upon because of its known strong nonlinear optical properties. Numerous measurements on C_{60} showed the effectiveness of the setup in determining the nonlinear absorption coefficient. As an indication of the versatility of the setup, measurements were also performed on single crystalline ZnO. This was done in order to prove that the setup could handle different types of samples. This was then illustrated when the nonlinear properties of ZnO were measured.

Recommendations for future work

Future work on the setup should include making the setup more versatile and more sensitive. Sensitivity can be improved by using lambda half plates as attenuators instead of neutral density filters. The laser light from the Dye laser is polarized and the lambda half plates can use this property to attenuate the beam by any value. Neutral density filters have fixed values which fixes the amount that the beam is attenuated. Lambda half plates will increase the range of energies at which the experiments are conducted and in this fashion improve the sensitivity. If it is decided that still more sensitive measurements are needed, then the spatial and temporal stability of the laser can be improved by operating in single mode. This can be done by inserting a Fabry-Perot etalon inside the laser cavity.

As was mentioned in Section 4.2, the Z-scan setup was constructed with the idea in mind that it could be used with an optically pumped parametric oscillator (OPPO) that is pumped by a frequency tripled Nd:YAG laser. The OPPO has the advantage that its wavelength can easily be tuned over a very large region. It differs in this respect from the Dye laser where it is necessary to change the dyes when moving between wavelength regions. This ease of tunability will enable wavelength dependence measurements of the nonlinear properties.

Furthermore, there are plans to incorporate fluorescence measurements with the Z-scan. By looking at how the fluorescence of a sample changes as a function of the intensity, it is possible to comment on the processes involved, namely whether two- or three-photon absorption is taking place or whether the nonlinear effects are dominated by scattering. This will increase the amount of information obtained from a sample and thus the versatility of the setup.

Appendix

Details, specifications and explanation of components used in experimental setup

XeCl Excimer laser:

Use: This laser is used to pump the Dye laser. It provides the excitation energy that the Dye laser requires to operate.

Specifications:

Make: Lambda Physik EMG 101 MSC

Wavelength: 308 nm

Energy: 100 mJ

Pulse Length: 16 ns

Repetition rate: Variable but set to 10 Hz for the experiments performed



Dye laser:

Use: The Dye laser was the laser used for all the experiments. It provided the laser light of sufficient intensity to observe the nonlinear effects in the investigated samples. It also allowed for tunability in wavelength.

Specifications:

Make: Lambda Physik FL3001

Wavelength: Variable but set to 540 nm for C₆₀ and ZnO investigations.

Energy: Variable and attenuated with NDFs to the μJ range

Pulse Length: 10 ns

Repetition Rate: 10 Hz (Determined by Excimer laser)

Fast photodiode

Use: The fast photodiode is used to trigger the Boxcar integrator and the oscilloscope. It was placed in such a manner that it would collect some of the Excimer laser's reflected light. It thus allows for the synchronization of the setup.

Specifications:

Make: Thorlabs DET210

Type: Si PIN

Rise Time: 1 ns

Active Area: 0.8 mm²

Spectral Range: 200 - 1100 nm

Neutral density filters (NDF)

Use: The Neutral Density Filters are inserted in the laser beam to attenuate the laser energy in order to obtain the desired energy with which the experiments are to be performed. They are also used to protect the detectors (which are sensitive photodiodes) from saturation and damage.

Specifications:

Make: Edmund Industrial Optics

Optical Density Values: 0.3; 0.5; 1.0; 1.3; 1.5; 2.0; 2.5; 3.0

Lens (L)

Use: The lens is used to focus the beam onto the sample, creating the tight focusing geometry required by the theory of the Z-scan experiment.

Specifications:

Make: Newport

Focal Length: 100 mm

Cuvette (sample holder)

Use: The liquid samples are placed in the high quality quartz cuvette when analyzed

Specifications:

Make: Starna

Optical Path Length: 2 mm

Material: Spectrosil Quartz

Transmission region: 170 nm - 2700 nm

Large area photodiodes (LAPD)

Use: The large area photodiodes are used as the detectors, both probe and reference, in the experiment because of their high sensitivity at low energies.

Specifications:

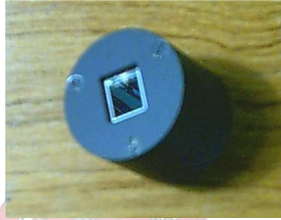
Make: Thorlabs FDS1010

Type: Si PIN

Rise Time: 45 ns

Active Area: 94.1 mm²

Spectral Range: 400 nm - 1100 nm



Large area photodiode in housing.

Large area photodiode power supply

Use: The large area photodiodes power supply was built in house for supplying a DC bias voltage to the large area photodiodes.

Specifications:

Make: Self built

Voltage Range: Voltage variable from 0 - 15 V

Translation stage with stepper motor (TS)

Use: The translation stage with stepper motor is used to move the sample under investigation along the Z-axis of the laser beam during the experiment.

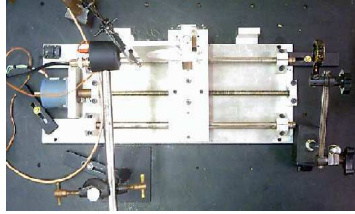
Specifications:

Make: Superior Electric

Total range 280 mm

Resolution: 200 steps per revolution

Distance per revolution: 2.508 mm



Translation stage with stepper motor

Stepper motor driver

Use: The stepper motor driver is the interface between the computer (PC) and the stepper motor on the translation stage. It controls the movement of the stepper motor based on the commands received from the computer.

Specification:

Make: Self built

Settings: Set to micro-step the stepper motor in order to double the resolution to 400 steps per revolution



Translation stage driver.

Translation stage power supply

Use: Provides the power for both the stepper motor and the stepper motor driver.

Specifications:

Make: Standard desktop computer power supply

Computer (PC)

Use: The computer is the heart of the experiment. It is responsible for the automation of the experiment. It controls the movement of the stepper motor, the data acquisition, the data analysis and processing.

Specifications:

Processor: Intel Celeron 300 MHz

Memory: 256 MB RAM

Data Acquisition Card

Make: PCI 726 Data Acquisition Card from Eagle Technology

Specifications:

16 SE or 8 Diff A/D Channels

14 bit Analog Resolution

100 kHz A/D Sampling Rate

4 x 14 bit D/A Channels

24 (3 x 8) DIO Channels

3 x 16 bit Counter Timers (User)

3 Interrupt Sources (PCI-730/726)

2048 FIFO buffer with programmable word count

DB25M (A/D & D/A); IDC40 (DIO) Connectors

Windows98/ME/2000/XP (NT on request)

Linux OS Support

WaveView for Windows Data Acquisition & Logging Software

Labview, Testpoint & Agilent-VEE

Supplied with EDR Enhanced Software and Internal Cable with PC bracket

(IDC40 to DB37)

Software:

Labview 7.0: Used for the control of the stepper motor, the data acquisition and the processing of the data in order to extract the nonlinear absorption coefficient.

MatLab 6.0: Used for filtering the rough data and performing the statistics necessary to determine the error on the measurements.

Gated integrator and Boxcar averager (BC)

Use: The boxcar integrator enables the capture of the peak value of extremely fast pulses which cannot be measured by conventional data acquisition methods.

Specifications:

Make: Stanford Research Systems SR250

Gate widths from 2 to 15 μs (expandable to 150 μs)

Internal rate generator

Active baseline subtraction

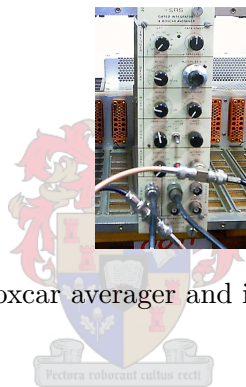
Shot-by-shot output

Gate output for precise gate timing

Average 1 to 10,000 samples

DC to 20 kHz repetition rate

Low jitter ($<20 \text{ ps} + 0.01\%$ of delay)



Boxcar averager and integrator.

Oscilloscope

Use: The oscilloscope is used to inspect the signal from the detectors and the boxcar integrators visually. This allows for the adjustments on the boxcar integrators to ensure correct overlap of the boxcar's gate and the signals from the large area photodiodes. The output from the boxcars can also be checked to ensure that the data acquisition card is not saturated or damaged.

Specifications:

Make: Tektronix TDS 3034

Nr Channels: 4

Bandwidth: 300 MHz

Sample Rate: 2.5 GS/s

Bibliography

- [1] Milonni P.W. and Eberly J.H. (1988). "*Lasers*", Chapters 2, 8, 14, 17, 18. John Wiley and Sons, New York.
- [2] Steinmann C.M. (1999). *Development and characterization of a tunable laser source in the vacuum ultraviolet*. MSc. Thesis, University of Stellenbosch, South Africa.
- [3] Boyd, R.W. (1992). "*Nonlinear Optics*", Chapter 2. Academic Press, London.
- [4] Scheidt, T. (2001). *Generation von solvatisierten elektronen in alkoholen*. Diplomarbeit, Technische Universität München, Deutschland.
- [5] Sheik-Bahae M., et al (1990). *Sensitive Measurement of Optical Nonlinearities Using a Single Beam*, IEEE Journal of Quantum Electronics, Vol. 26, No. 4, pp. 760-768.
- [6] Sheik-Bahae M., Said A.A. and Van Stryland E.W. (1989). *High-sensitivity, single-beam n_2 measurements*, Optics Letters, Vol. 14, No. 17, pp. 955-957.
- [7] Weaire D., et al (1979). *Effect of low-power nonlinear refraction on laser-beam propagation in InSb*, Optics Letters, Vol. 4, No. 10, pp. 331-333.
- [8] Rhee B.K., Byun J.S. and Van Stryland E.W. (1996). *Z-scan using circularly symmetric beams*, Journal of the Optical Society of America, Vol. 13, No. 12, pp. 2720-2723.
- [9] Taheri B., et al (1996). *Intensity scan and two photon absorption and nonlinear refraction of C_{60} in toluene*, Applied Physics Letters 68 (10), pp. 1317-1319.
- [10] Olivier T, Billard F and Akhouayri H. (2004). *Nanosecond Z-scan measurements of the nonlinear refractive index of fused silica*, Optics Express, Vol. 12, No. 7, pp. 1377-1382.

- [11] Couris, S., et al (1995). *Concentration and wavelength dependence of the effective third-order susceptibility and optical limiting of C_{60} in toluene solution*, Journal of Physics B: Atomic, Molecular and Optical Physics 28, pp. 4537-4554.
- [12] Scheidt, T. et al (2004). *Optical second harmonic imaging of zinc oxide thin films grown by metal organic chemical vapour deposition (MOCVD)*, Physica Status Solidi (c) 1, No. 9, pp. 2243-2249.
- [13] Kroto, H.W., et al (1985). Nature 318, 162.
- [14] Picture of C_{60} molecule showing a plane of electrons. Available at: URL:<http://www.chem.swin.edu.au/test/data/smallball.jpg>. Accessed October 14, 2004.
- [15] Kost, A. et al (1993). *Optical Limiting with C_{60} in polymethyl methacrylate*, Optics Letters Vol. 18, No. 5, pp. 334-336.
- [16] McLean, D.G., et al (1993). *Nonlinear absorption study of a C_{60} -toluene solution*, Optics Letters Vol. 18, No. 11, pp. 858-860.
- [17] Marciu, D.(1999). *Optical Limiting and Degenerate Four-Wave Mixing in Novel Fullerenes*, PhD Thesis, Virginia Polytechnic Institute and State University, Blacksburg, VA, USA.
- [18] Couris S. et al (2003). *An experimental investigation of the nonlinear refractive index (n_2) of carbon disulfide and toluene by spectral shearing interferometry and z-scan techniques*, Chemical Physics Letters 369, pp. 318-324.
- [19] Aranda, F.J. et al (2000). *Optical Limiting in Hydrothermal Zinc Oxide Crystals*, available at URL:<http://www.afrlhorizons.com/Briefs/0001/SN9912.html>. Accessed February 26, 2004.
- [20] Najechalski, P. et al (2001). *Two-photon absorption spectrum of poly(fluorene)*, Chemical Physics Letters 343, pp. 44-48.